

Wearable UV Detector for Real Time UV Index Monitoring

By

Adnin Tazrih Natasha

A Thesis Submitted to Macquarie University

For the Degree of Master of Research

School of Engineering

July 2022



MACQUARIE
University
SYDNEY · AUSTRALIA

Examiner's Copy

Statement of Originality/Candidature

I, Adnin Tazrih Natasha, declare that this report, submitted as part of the requirement for the award of Master of Research in Engineering from the School of Engineering, Macquarie University, is entirely my own work unless otherwise referenced or acknowledged. This document has not been submitted for qualification or assessment at any academic institution.

Student's Name: Adnin Tazrih Natasha

Student's Signature: Adnin Tazrih Natasha

Date: 15/07/2022

Statement of Covid-19 Impact

The impact of Covid-19 is terrifying around the globe. Every sector of the country has been affected and suffered a great loss. The after effect of Covid-19 is far worse. I, Adnin Tazrih Natasha, student at Macquarie University, Sydney, Australia studying Master of Research in Electronics Engineering has been a victim of Covid-19 and affected severely. I started my journey of research in mid-way of Covid-19 wave and was studying and working on my project from home. Due to social distance guidelines and immense outbreak of the deadly virus I had to perform experiments from home from August 2021 to January 2022 and after coming back to the campus, I got infected by Covid-19 in March 2022. I suffered awfully from the virus infection and my research work got more delayed. During my research study period I was only able to work for 4 months in the laboratory for my project and the rest 5 months at home. It was hard for me to finish my work on time and work on the electrical part of the project from home. Still, I am grateful that I survived the virus and during my study my supervisors, my friends and my family supported me massively.

Acknowledgement

With earnest and profound gratitude, I would like to acknowledge and oblige to my Supervisor Dr. Noushin Nasiri and Co. Supervisor Dr. Binesh P Veetil. Dr. Noushin Nasiri is guiding the research project and assisting in various aspect in the progress of the project. The completion success of this project has been planned wisely and progressing with the proper direction from my Supervisor and Co. Supervisor Dr. Binesh P Veetil, for whose additional supervision is highly appreciable. I would also like to acknowledge the support and co-operation of my colleagues during my work.

Common Abbreviations

UV – Ultraviolet Rays

UVA – Ultraviolet A

WHO - World Health Organisation

BCC - Basal cell carcinoma

SSC - Squamous cell carcinoma

PAF – Population Attributable Fraction

BLE - Bluetooth low energy

DNA - Deoxyribonucleic Acid

CCDs - Charged coupled devices

LSPR - Localized surface plasmon resonance

ALD - Atomic layer deposition

MBE - Molecular beam epitaxy

CVD - Chemical vapour deposition

PLD - Pulsed laser deposition

RF - Radio frequency

FSP -Flame spray pyrolysis

IDE - InterDigitated Electrodes

EIS - Electrochemical impedance spectroscopy

LiPo - Polymer Lithium Ion Battery

SPDT – Single pole double throw switch

MSM - metal – semiconductor – metal

NWs – Nanowires

NPs – Nanoparticles

NTs – Nanotubes

NBs – Nanobelts

NFs – Nanoflakes

QDs – Quantum dots

NRs – Nanorods

TCO - Transparent conductive oxide

Common Nomenclature

CFCs – chlorofluorocarbons

CCl_4 - carbon tetrachloride

CH_3CCl_3 - methyl chloroform

HBFCs - hydrobromofluorocarbons

CH_3Br - methyl bromide

CH_2BrCl - bromochloromethane

eV - electron volts

TiO_2 - Titanium Dioxide

SnO_2 - Tin Oxide

GaN - Gallium Nitride

InN - Indium Nitride

SiC - Silicon Carbide

ZnO - Zinc Oxide

H - hydrogen(H),

F - fluorine (F),

In - indium (In),

Al - aluminium (Al)

$^{\circ}\text{C}$ – Celsius Temperature

Abstract

This thesis presents the successful development of an Ultraviolet (UV) index monitor for determining daily exposure of an individual under Sunlight. The core measurement of the UV index of the device is the calibration of the effect of incident sun rays on the UV nano sensor. The nano sensor is made of ZnO nanoparticles with an average particle size of 15 nm. It has been fabricated in the laboratory by flame spray pyrolysis fabrication technology which is based on the deposition and self-assembly of ultrafine nanoparticles on a water-cooled substrate. The UV nano sensor is fabricated on glass substrate with a dimension of 10 x 6 x 0.75 mm, featuring platinum interdigitated electrode. The device connects through Bluetooth low energy 5.0 communication to mobile application known as “UV Index Monitor”. The calculation of the UV index varies from a range of 1-10, where 1 stand for safe UV radiation and 10 stands for harmful exposure of UV. The mobile application connected to the device display alert messages to end users like, “You are safe”, “UV protection required” etc varying the range of UV in between 1 to 10. The device is designed in wearable watch frame structure. The device measurements are 5 cm in length, 3 cm in width and 2 cm in thickness. The power source of the device is 3.7 V rechargeable battery. The UV index data from the mobile application comes with sharing through emails or other platforms for data storage. These data can be further used for individuals’ medical health records.

Table of Contents

Statement of Originality/Candidature	ii
Statement of Covid-19 Impact	iii
Acknowledgement	iv
Common Abbreviations.....	v
Common Nomenclature.....	vi

List of Figures.....	ix
----------------------	----

List of Tables	ix
----------------------	----

Chapter 1 – Introduction	2
1.1 Aims and Objective.....	3
1.2 Project Scope.....	4
1.3 Chapters	4
Chapter 2 - Background and Literature.....	7
2.1 UV Sensitive Materials	8
2.1.1 Titanium Dioxide (TiO ₂).....	9
2.1.2 Tin Oxide (SnO ₂)	10
2.1.3 Diamond.....	11
2.1.4 Gallium Nitride (GaN)	12
2.1.5 Indium Nitride (InN).....	13
2.1.6 Silicon Carbide (SiC).....	14
2.1.7 Zinc Oxide (ZnO).....	15
2.1.7.1 Conventional Zinc Oxide (ZnO) MSM based UV photodetector:.....	15
2.1.7.2 Schottky UV photodetector:.....	16
2.1.7.3 p – n junction-based UV photodetector:	16
2.1.7.4 Homojunction photodiode:	16
2.1.7.5 Heterojunction photodiode:.....	17
2.2 Fabrication Technology	17
2.2.1 Thin film deposition:.....	18
2.2.2 Lithography:.....	19
2.2.3 Physical and Chemical Etching:	20
Chapter 3 – Materials, Devices and Methods	23
3.1 Materials.....	23
3.2 Mechanism, Apparatus, contents	23
3.3 Method	23
3.4 Sensor Testing Apparatus	24
Chapter 4 – UV Sensor System.....	28
4.1. Electronic components	28
4.1.1 Arduino Nano 33 BLE Sense:.....	29
4.1.2 Resistor:	31
4.1.3 Polymer Lithium Ion Battery (LiPo):.....	31
4.1.4 Adafruit Micro Lipo w/MicroUSB Jack - USB LiIon/LiPoly charger - v1	31
4.1.5 SPDT slide switch:.....	32
4.1.6 Vivo Android 12 smartphone:.....	32
4.2 Device Design	32
4.3 Mobile Application	35

Chapter 5 – Results and Discussions	38
5.1 Sensor Testing Results	38
5.2 Indoor Testing	42
5.3 Outdoor Testing	43
Chapter 6 - Conclusion	48
Chapter 7 – Future Work	50
REFERENCE.....	51
APPENDIX – I.....	54

List of Figures

1. Figure 1.1 Spectral Irradiance versus wavelength graph [3]	2
2. Figure 1.2 A visual of skin types and their UV sensitivity, tendency to burn, and skin cancer risk [5]	3
3. Figure 2.1 Photo response characteristics under (a) UV-A, (b) UV-B, (c) UV-C, and (d) 5 V bias with (e) showing the sensitivity and (f) responsivity of the photodetector based on SG-TiO ₂ [15]	10
4. Figure 2.2 (a) Cross-sectional SEM image of 3D SnO ₂ nano array; (b) Spectral response of the device; (c) I-V curves under different wavelengths and dark conditions; (d) Time–response curve of the device. [16].....	11
5. Figure 2.3 Photoresponse of the graphene/nanoporous GaN UV photodetectors.	12
6. Figure 2.4 Illumination intensity-dependent (a) photocurrent, (b) photosensitivity, (c) photoresponsivity, and (d) specific detectivity of Ag/GaN/InN/Ag heterointerface photodetector under the illumination of 266 nm, 532 nm, and 1064 nm lasers. [7]	13
7. Figure 2.5 The photocurrent-time plots of the flexible SiCNW-UVPD before and after 100 bending cycles at 10 V bias voltage.[19]	14
8. Figure 2.6 (a) Schematic of MSM photodetector [22], (b) Schematic of 2D palladium diselenide PdSe ₂ /GaN Schottky junction device [23], (c) Device Structure for ZnO thin films for p–n junction-based visible-blind ultraviolet photodetectors [24]	15
9. Figure 2.7 Nanoparticles evolution in FSP technique [27].....	19
10. Figure 2.8 Photolithography Process [30].....	20
11. Figure 2.9 Etching profiles generated with (a) isotropic etching, (b) dry anisotropic etching, and (c) wet anisotropic etching [29].....	21
12. Figure 3.1 (a) FSP Fabrication process, and (b) Thin-film Platinum InterDigitated Electrode (5/5 μm) [32]	24
13. Figure 3.2 (a) Thorlabs Laboratory modular optical tweezer setup, (b) Black box light setup, (c) DC2200 - High-Power 1-Channel LED Driver with Pulse Modulation, 10.0 A Max, 50.0 V Max [33] and (d) Keithley 2450 – Source Meter Instrument (200 V, 1 A, 20 W) [33].....	25
14. Figure 4.1 (a) Arduino Nano 33 BLE Sense pinout diagram and (b) different sensor on the board. [34].....	29
15. Figure 4.2 (a) Resistor, (b) Lipo battery, (c) Lipo battery type C charger and (d) SPDT slide switch.....	31
16. Figure 4.3 (a) UV index monitor device circuit and, (b) practical implementation of the circuit in a compact device structure.....	33
17. Figure 4.4 UV index monitor device connection diagram.....	34

18. Figure 4.5 a. UV Index Monitor mobile application, b. UV index monitor user interface, c. Application data history and d. calendar chart for the data.....	35
19. Figure 5.1 mcte1-19913l-s peltier module, 200w, 50 x 50 x 3.5mm [50]	38
20. Figure 5.2 Resistance versus Time graphs at different temperature of a) 25°C, b) 30°C, c) 35°C and d) 40°C, at the light density of 20mA, 40mA,80mA and 150mA, respectively.....	39-40
21. Figure 5.3 Effect of Temperature on the sensor at the light density of 20mA, 40mA,80mA and 150mA, respectively.....	41
22. Figure 5.4 Digital Ultraviolet Radiometer model 6.5 [51].....	42
23. Figure 5.5 Comparison of UV index results from this device and Digital Ultraviolet Radiometer under Thorlabs light setup in the laboratory.....	43
24. Figure 5.6 UV Index Monitor	44
25. Figure 5.7 a.7 days outdoor UV index by this device and b. Outdoor Comparison with Commercial UV Radiometer	45

List of Tables

1. Table 2.1 - Types of UV Radiation [8].....	7
2. Table 3.1 – LED current and Light Density	26
3. Table 4.1 – Electronic Components used in the UV sensor system.....	28
4. Table 4.2 – Technical Specification of Arduino Nano 33 Ble Sense [34].....	29
5. Table 5.1 – Peltier Module Temperature calibration chart	39
6. Table 5.2 – UV Index Numerical Indicator	42
7. Table 5.3 – Weather of 7 Consecutive Days of outdoor testing in Sydney (H = Highest, L= Lowest) [44].....	46

Chapter One

Introduction

Chapter 1 – Introduction

Ultraviolet radiation (UV) is a non-ionizing form of radiation emitting from the Sun and artificial sources, such as mercury vapour lighting, tanning beds, and some lasers [1]. The oxygen in the Earth's atmosphere absorbs the majority of UV radiation from sunlight, creating the ozone layer in the lower stratosphere. Nearly 99 percent of the UV energy that does reach the surface of the Earth is UVA radiation [2].

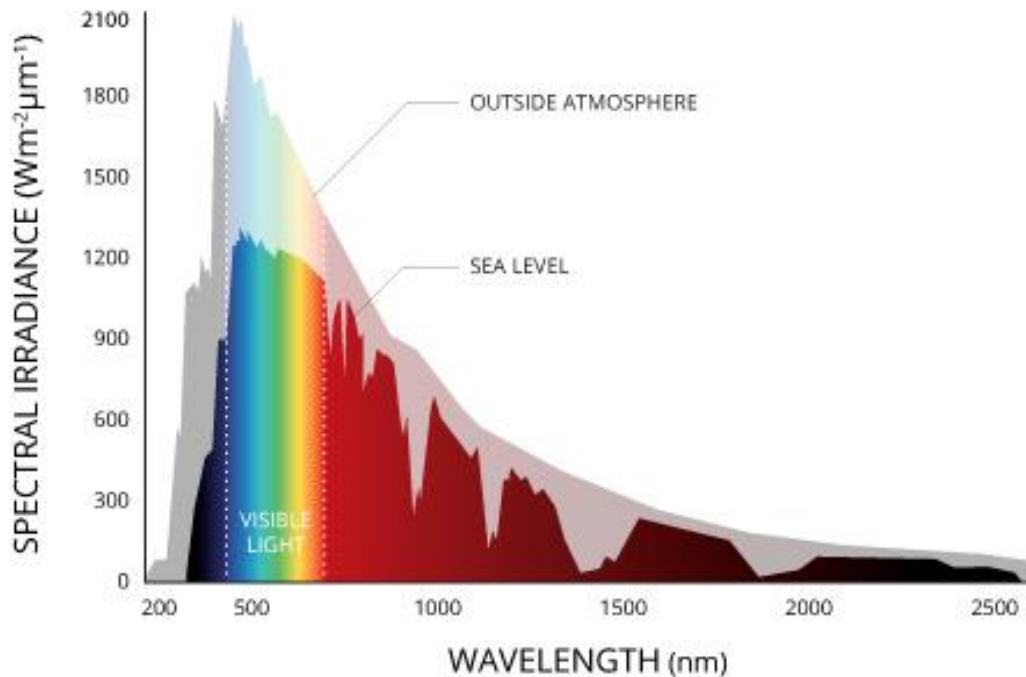


Figure 1.1 Spectral Irradiance versus wavelength graph [3]

UV radiation is necessary for human skin to produce Vitamin D which is required for our metabolism [4]. Vitamin D helps the body bone development through absorbing calcium and phosphorus from food [4]. It is recommended by World Health Organisation (WHO) to have daily exposure to sunlight for 5 to 10 minutes at least 2 to 3 times on a weekly basis [1]. It can be used as therapeutic agent for disease like psoriasis [2]. However, over exposure to UV radiation could cause severe health risks such as skin cancer, sunburn etc [1]. Sunburn is regarded as short-term effect of over exposure of UV radiation which causes the skin burns and causes itchiness [1]. Skin cancer, premature aging and eye diseases are the long-term effect of UV over exposure. UV radiation has lower penetration power unlike X-rays [2]. For this reason, it has direct effect on the human skin surface, where it results in sunburn, suntan, carcinogenic changes and furthermore it develops melanoma, a type of skin cancer in the skin cell called melanocytes.

Melanin is a chemical pigment in the human body that absorbs UV and reduces penetration into tissues [4]. People with skin type from 1 to 3 [1.2] usually have less melanin pigment and consequently, are more

vulnerable to overexposure to UV radiation. Aging, wrinkling, thickening, blisters, swelling, seepage of fluid, sloughing of the skin surface and changes in skin pigmentation are other added effects of UV radiation.

UV radiation can reach to human through various sources like directly from sun, scattered open sky, reflected from the environment, which means even if a person is under shade is also likely to get exposed to UV. To reduce the risk of the harmfulness effect of UV radiation, it is necessary to monitor the radiation dosage on a daily basis using smart sensing technologies.

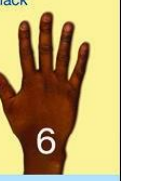
NATURAL SKIN COLOUR	Very fair, pale white, often freckled	Fair, white skin	Light brown	Moderate brown	Dark brown	Deeply pigmented dark brown to black
						
UV SENSITIVITY & TENDENCY TO BURN	Highly sensitive Always burns, never tans	Very sensitive Burns easily, tans minimally	Sensitive Burns moderately, usually tans	Less sensitive Burns minimally, tans easily	Minimal sensitivity Rarely burns	Minimal sensitivity Never burns
SKIN CANCER RISK	Greatest risk of skin cancer	High risk of skin cancer		At risk of skin cancer	Skin cancers are less common, but are often detected at a later, more dangerous stage. Increased risk of low vitamin D levels.	

Figure 1.2 A visual of skin types and their UV sensitivity, tendency to burn, and skin cancer risk [5]

1.1 Aims and Objective

Australia is having the highest rates of developing skin cancer in the world [6]. According to the Cancer Council Australia, 2 out of 3 Australians will be diagnosed with skin cancer by the age of 70 [6]. There are three main skin cancers including Basal cell carcinoma (BCC), Squamous cell carcinoma (SCC) and melanoma [6]. Among them, melanoma is the least common but most severe form of skin cancer with 16,878 new cases of melanoma being detected in Australia in 2021 [4,6]. According to the Australia Cancer Council, almost a million non-melanoma skin cancer patients receive therapy annually [6]. The signs of non – melanoma skin cancers are glossy, pale, or bright pink lump on the skin, the skin may become inflamed, bleed, and ulcerate and it may even seem to heal before re-inflaming [6]. Melanoma frequently has no symptoms, but the first indication is either a change in an already-existing mole or the emergence of a new lesion [6]. Exceptional melanomas can develop under the nails, on the palms of the hands or feet, or in areas of the skin or body that have never been exposed to sunlight which is also known as ocular melanoma [6]. There are preventions and treatments available for skin cancer such as surgery, radiation therapy, chemotherapy, photodynamic therapy, immunotherapy, sunscreen, or lotion with high Sun Protection Factor (SPF). Alongside treatments and preventions, monitoring and regulation of daily UV radiation could be helpful to acknowledge the right protection and can be added to individual health record.

The aim of this project is to design and develop a wearable UV monitoring device capable of real-time monitoring of UV index to promote Sun safety. The core functionality of this device will depend on the capability of the nano sensor and the amount of UV radiation absorbed by the sensor. Hand watch has been considered as model for the UV Index monitoring device because of the comfort of wearing the device on the body. The wrist is suitable for mounting or binding the UV index monitoring device with straps and it will be exposed to sunlight as much as possible. The UV index will be displayed in the mobile application built based on the Bluetooth low energy (BLE) connectivity of the Arduino Nano 33 BLE Sense. The mobile application will show the user UV index alongside temperature and humidity at real time. The user interface has been made simple with clear background and alert messages for the end users and data sharing option with 7 days data details periodically.

1.2 Project Scope

The treatment and preventions of skin cancer caused by UV radiation is documented after an individual is diagnosed with it, but the impact on a person's daily health is frequently not recorded. The motivation behind this project is to design a device that can communicate with a mobile platform to track and record a person's frequent exposure to UV radiation. The project is based in Australia as it is mentioned earlier that Australia is leading in skin cancer [6]. The project has been carried out within 8 – 10 months' time frame.

The scope of the study is to provide real-time monitoring of UV index using a smart wearable device equipped with super sensitive UV nano sensor. The companion app developed for this device is designed to communicate the measured UV radiation using UV index values on a scale of 1-10, with UV index of 1 being the lowest and 10 being the highest UV level. The value of UV index will be displayed on the mobile app enabling the end user to moderate their exposure to UV radiation. The app will also provide the end user with the data storage option for further analysis and review.

1.3 Chapters

In this section, the overall chapters of the papers will be briefly described according to the appearance in the paper. Below in the chapter wise discussion:

Chapter – 1 Introduction

The chapter provides UV identification and basic theory, with a focus on the alarming issue of UV over exposure on human health. It brings out the factors that has been controlled and needs to be furthermore

developed to be 100 percent successful in preventing UV negativity upon human body. The chapter provides information on the technologies used for the device which will be describe in more details in the upcoming chapters.

Chapter – 2 Background and Literature

The chapter will contain information about background and literature on UV sensor fabrications and materials. The chapter will discuss different fabrication technique and UV sensitive materials.

Chapter – 3 Materials and Methods

The chapter will describe the materials and nanofabrication technique used in this research and will discuss the process in detail.

Chapter – 4 UV Sensor System

The chapter will talk about the electronical concept of the device design. It will describe the connections, setups and electronic components used for building the UV monitoring device and designed mobile application for the device.

Chapter – 5 Results and Discussion

The chapter will show results obtained with device with comparison of the Laboratory setup of measurement and discuss on the outcome of the Research.

Chapter – 6 Conclusion

This chapter will discuss the successful development of the wearable UV index monitoring device and its potential contribution in medical field.

Chapter – 7 Future Work

This chapter will discuss the possible future works that can be taken into consideration.

Chapter Two

Background and Literature

Chapter 2 - Background and Literature

In definition, UV radiation is an electromagnetic radiant wave form energy emitted with a wavelength varying from 10 nanometre (nm) to 400 nm [8]. Electromagnetic radiation consists of waveforms generated by the electromagnetic field, propagating through space with electromagnetic energy [9]. The waveforms that propagate with electromagnetic radiations are radio waves, microwaves, infrared, visible light, UV, X-rays, and gamma rays forming electromagnetic spectrum [9]. UV radiation naturally originates from the sunlight, constituting 10 percent of the entire electromagnetic radiation output from the sun [8]. It is possible to produced UV artificially on the earth surface. On one hand, the non-ionizing radiation characteristics of long length UV is often used for fluorescing lighting, interactions with organic molecules etc. [8]. On the other hand, short wavelength UV damages Deoxyribonucleic Acid (DNA) of living beings and sterilizes the surface in contact and hence results in sunburn, suntan, and types of skin cancer for human being [8]. As UV is harmful for human body, it needs to be observed frequently. The Table 2.1 will present all three types of UV radiation with their wavelength range and characteristics. **The types of UV and which one is harmful and needs to be watched.**

[Table 2.1](#) - Types of UV Radiation [8]

UV Radiation	Wavelength(nm)	characteristics
UVA	315 -400	Does not get absorbed by the ozone layer
UVB	280 -315	Partially absorbed by the ozone layer, thus some portion of it reaches the earth surface
UVC	200 -280	Completely absorbed by the ozone layer and the atmosphere

UV radiation on the earth surface depends on different factors, such as the position of the Sun in the sky, height of the Sun from the earth surface at exact position, latitude, presence of cloud, altitude, the thickness of the ozone layer and ground reflection [9]. Ozone layer is the lower part of earths stratosphere that absorbs most of the suns biologically harmful UV radiation [10]. Increase amount of human made pollution causes decaying of the ozone layer and in return the UV Radiation reaches the earth surface in abundant [9]. This reductions in the ozone layer passing harmful portion of the UV Radiation causes impact on human heath, animals, marine organisms and in green nature.

Atmospheric data demonstrates that uses of ozone depleting substances like chlorofluorocarbons (CFCs), halons, carbon tetrachloride (CCl₄), methyl chloroform (CH₃CCl₃), hydrobromofluorocarbons (HBFCs), hydrochlorofluorocarbons (HCFCs) methyl bromide (CH₃Br) and bromochloromethane (CH₂BrCl) on the

earth surface releases chlorine and bromine atoms are making ozone layer thinner in the stratosphere by destroying ozone molecules [11]. This ozone layer depletion contributes to varying extents on the global warming. During 1974 chemists Mario Molina and Frank Sherwood Rowland put light on the depletion of the ozone layer gradually by studying the links between the CFCs gases and the ozone layer breakdown [11]. The ozone layer depletion is noticed in two ways around the earth surface [11]. The first mid ozone layer depletion is in the mid latitude over Australia. Data collection from the upper layer of the atmosphere shows that there has been gradual decaying of the ozone layer all around the world, which makes the ozone layer depletion over the Australian continent by 5 to 9 percentage since the 1960s century [11]. This incident serves the reason for the Australian to be more or overly exposed to UV and Australia leading the way to life threatening skin cancer. The second depletion way of the ozone layer is around the Antarctica and to some extent of the Arctic continent where the ozone layer in spring is so thinned to resulting in an 'Ozone Hole' [11]. Department of Agriculture, Water and the Environment sector of Australian Government has stated that improve the condition of the depletion in the ozone layer, Australia has an international agreement with other countries known as ozone protection and synthetic greenhouse gas management act 1989 by decreasing uses of the ozone depletion substance in the nature.

For daily monitoring of UV, internationally accepted standardised UV Index has been developed which is an open-ended numerical scale starting from 0 to 11+ with no limit in the upper scale. Where 0 means no radiation detected and 11+ means extreme condition of UV radiation detected [12].

2.1 UV Sensitive Materials

The noteworthy development of nano structuring of wide bandgap semiconductors have widened the progress of developing UV detection with great survival nature in difficult weather condition with a low – cost production and performance much satisfactory than cost effective conventional equipment. In definition, materials in between conductors and insulators or non-conductors are semiconductors. It is confined of pure elements like silicon, which conducts electricity more than an insulator (i.e., glass) but less than a pure conductor (i.e., copper or aluminium). Wide-bandgap properties of semiconductor permits electronical devices to operate at higher voltages, frequencies, and temperature than conventional semiconductor. It has got higher bandgap around 2 electron volts (eV). UV detection traditionally has been acquired by photomultiplier tubes (PMTs), thermal detectors, narrow bandgap, semiconductor photodiodes or charged coupled devices (CCDs) [13]. These devices are bulky and fragile instruments with high power supplies [13]. Research studies has shown that UV photodetectors based on wide bandgap semiconductors like SiC, III nitrides, diamonds, and some II-V group semiconductors, such as ZnO and TiO₂ are more efficient than conventional semiconductors [13]. Wide bandgap semiconductors have been found popular in understanding of the UV detection fundamental process and prominent responsive behaviour to the UV

radiation [14]. There are some factors which controls the photo responsive behaviours of the wide bandgap semiconductor nano structured devices such as the grain size, processing condition, crystallographic orientation, the concentration defects, and the bandgap [14]. We will discuss about some wide bandgap semiconductors found promising by previous research for applications like chemical photo detection, environmental, biological analysis, monitoring fame, astronomical studies, optical communications, and radiation detection in this section below [14].

2.1.1 Titanium Dioxide (TiO₂)

Due to its exceptional chemical durability, thermal stability, and small size, TiO₂ is one of the most studied sensing materials for the creation of UV photodetectors. [15]. Anatase, rutile, and brookite are the three polymorphs of the wide bandgap semiconductor TiO₂ that are found in nature [15]. It is a well-known transparent conductive oxide (TCO) with suitability for UV detection against a background with infrared and visible light. The characteristics of TiO₂ are absolute bandgap of 3.2 eV for anatase and 3.0 eV for rutile, high refractive index, distinctive absorption, and low fabrication cost for which is it is one of the promising materials for photo detector [14]. The UV photodetector polymorphs anatase and rutile are often the most researched [15]. Rutile is more thermodynamically stable than anatase, however due to its large grain size and high electron-hole recombination rate, it is not a good material for UV photodetector performance [15]. Anatase is renowned for having tiny grains, which produce more surface areas and less surface energy, which qualifies it as a good candidate to make up for the UV photodetector deficit brought on by rutile [15]. In the research, “Characteristics and Sensing of Sol-gel derived Titanium Dioxide-based Ultraviolet Photodetector on Flame Retardant-4 Board”, Kai Ti Low *et al.* states in [Fig. 2.1](#)(a), (b) and (c), respectively, the photocurrent response of Sol – gel (SG)-TiO₂ based photodetectors under UV A, UVB, and UVC illuminations [15]. When switching between the on/off state of UV lights, the measured photocurrent density is steady during each cycle [15]. In [Fig. 2.1](#) (f) It is notable that UV-B and UV-C photo responses were lower than those of UV-A [15]. In both [Fig. 2.1](#) (e) and (f), a similar pattern was shown in the sensitivity of the photodetector, where the highest sensitivity was obtained when illuminated by UV-A, followed by UV-C, and then UV-B, where the highest sensitivity under all bias was obtained [15].

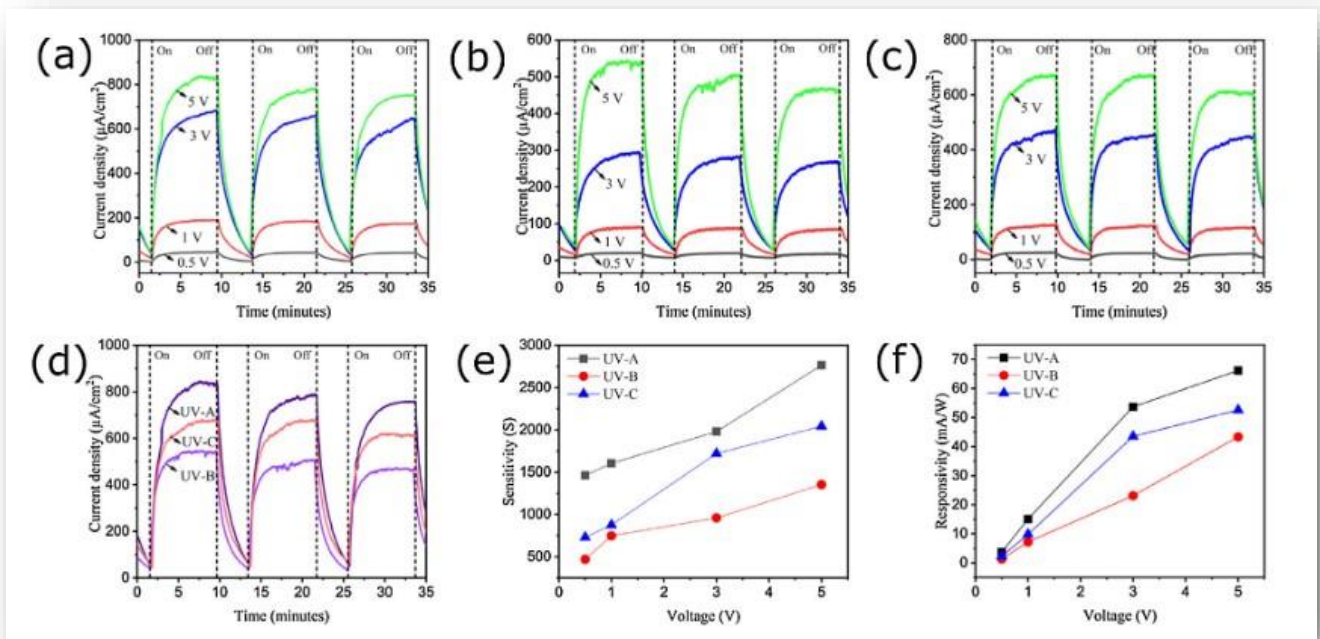


Figure 2.1 Photo response characteristics under (a) UV-A, (b) UV-B, (c) UV-C, and (d) 5 V bias with (e) showing the sensitivity and (f) responsivity of the photodetector based on SG-TiO₂ [15]

2.1.2 Tin Oxide (SnO₂)

SnO₂ is considered to be the most favourable semiconductor for UV spectrum detection or photodetector semiconductor material [16]. The bandgap of SnO₂ is 3.6 eV. SnO₂ has defects and dangling bonds in the structure which is remarkable in the light transmission and detection process [16]. The existence of surface electron traps and oxygen absorption makes the SnO₂ photodetectors more sensitive to UV radiation with a limitation of further improvement in the respond speed [16]. Qiannan Ye *et al.* in the “Research and Progress of Transparent, Flexible Tin Oxide Ultraviolet Photodetector”, mentioned that the results of the research in [Fig. 2.2](#) (b) depicts the photodetector's spectrum response to a constant light intensity of 1.0 V bias and in the UV area, the device had a clear photocurrent [16]. [Fig. 2.2](#) (c) depicts the photodetector's I-V curve at various wavelengths and in complete darkness and the device's dark current was just 2.3 pA at 1.0 V of bias, and it could produce a photocurrent of up to 0.5 nA when exposed to 350 nm light [16]. [Fig. 4d](#) displays the photodetector's time-response curve and the rising time and decay time were both under 0.3 seconds, as can be observed [16].

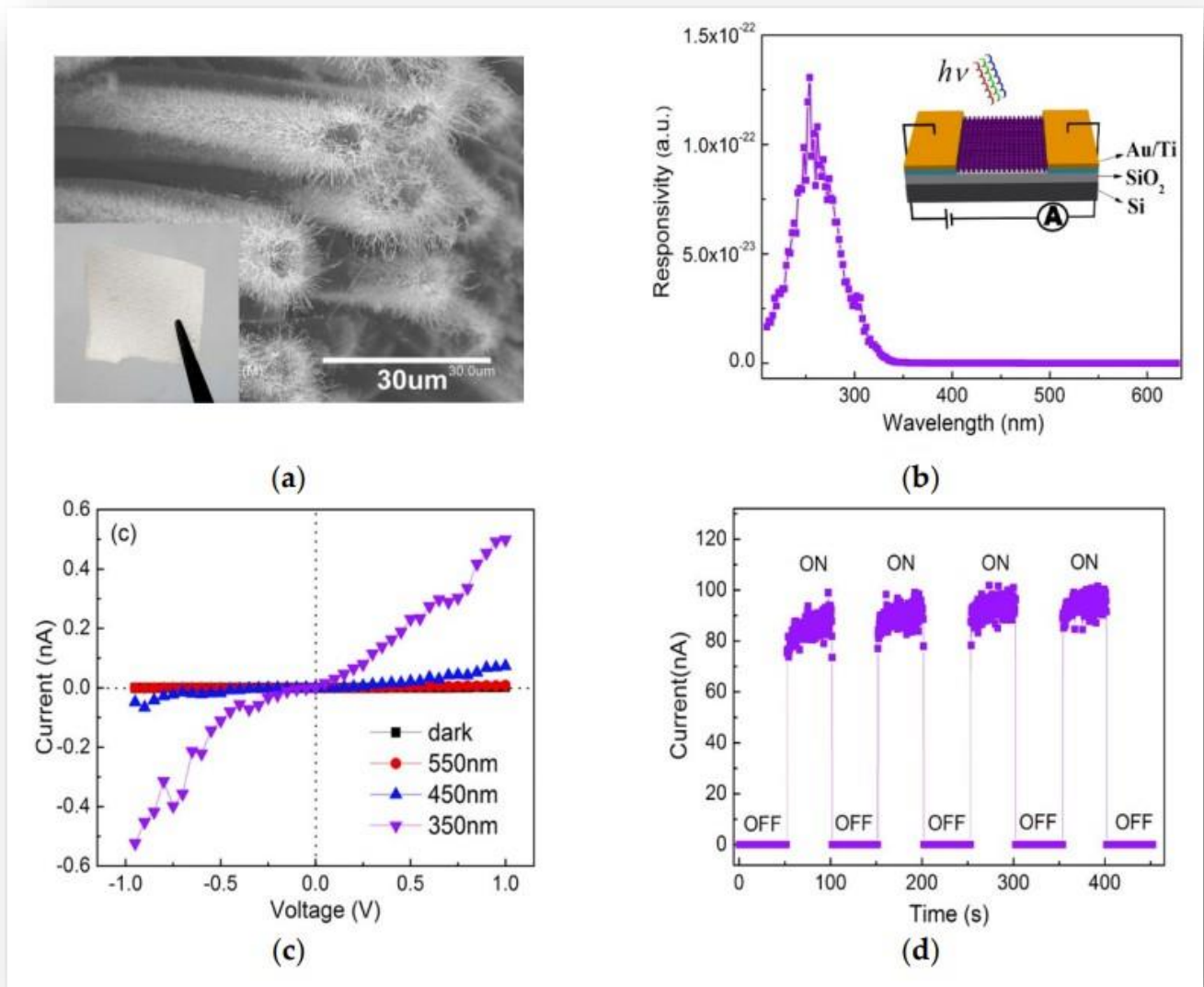


Figure 2.2 (a) Cross-sectional SEM image of 3D SnO₂ nano array; (b) Spectral response of the device; (c) I-V curves under different wavelengths and dark conditions; (d) Time–response curve of the device. [16]

2.1.3 Diamond

Diamond shows the characteristics of high thermal conductivity, saturation velocity, much higher carrier mobilities and the lowest dielectric constant of all the semiconductors with a wide bandgap of 5.5 eV [14] [17]. Diamond UV sensors are the first diamond thin-film devices available commercially [14]. The detectors have been proved successful in case of high energy particle, ionization detection, radiotherapy dosimetry, calibration of deep UV lithography and UV astronomy imaging [14]. The cost, size and variability of diamond makes it difficult in the competition with silicon [14].

2.1.4 Gallium Nitride (GaN)

The GaN saturation velocity is higher than GaAs and the optical phonon energies are three times larger than of GaAs [14]. GaN with a bandgap of 3.39 eV (366nm) in a room temperature has most promising nature for semiconductor photonic device operating in the UV spectrum areas [14]. Due to its inherent UV absorption window, high electron saturation drift velocity, exceptional radiation hardness, chemical and thermal stability, etc., GaN has been regarded as one of the most promising choices for UV photodetectors [18]. The high quality GaN with greater wavelength and transparency is the ideal material for photodetector devices and capable of not responding to the infrared and visible solar spectrum but maintaining efficiency in the UV quantum [14]. The huge surface-to-volume ratios and nanoscale confinement of the nanostructured GaN-based UV photodetectors allow for a significant boost in response and internal gain when compared to conventional thin film and bulk GaN [18]. Moreover, the super radiation hardness and high temperature resistivity of the GaN makes the fabricated devices more suitable for extreme conditions [14].

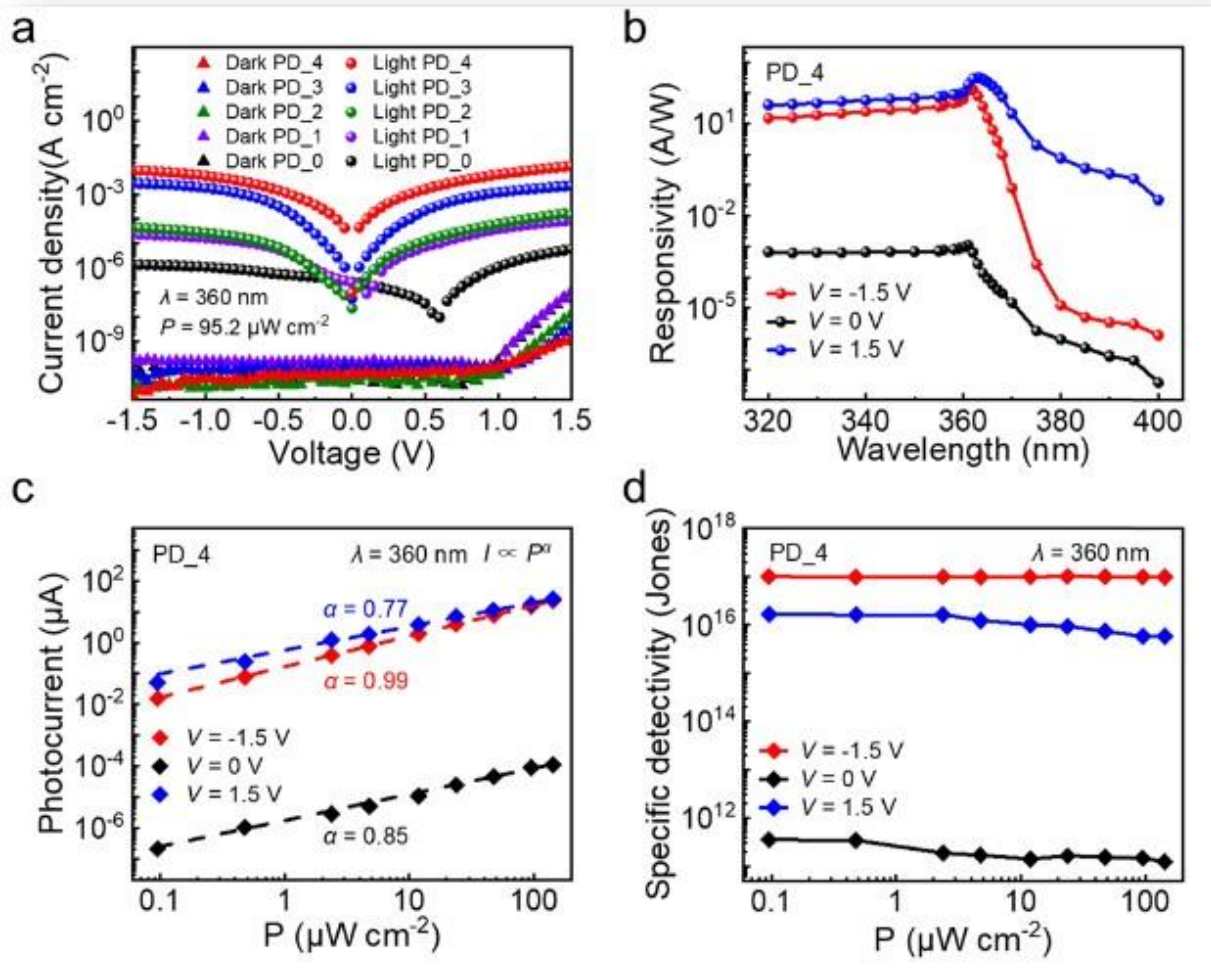


Figure 2.3 Photoresponse of the graphene/nanoporous GaN UV photodetectors.[18]

Recently Jing Li *et al.* developed Ultrahigh Sensitivity Graphene/Nanoporous GaN Ultraviolet Photodetectors, and the results of the research in the Fig. 2.3 depicts that the photo response of UV photodetectors can be greatly enhanced by converting bulk GaN into high porosity nano porous GaN [18].

2.1.5 Indium Nitride (InN)

InN is a very special material within the III-N family because of its short and direct bandgap of 0.64 eV, small effective mass of $0.04 m_0$, and strong electron mobility [7]. For applications involving high-frequency optoelectronic devices, these characteristics are desirable [7]. At room temperature, the theoretical limit for InN mobility is $14,000 \text{ cm}^2/\text{Vs}$. The thin-film structure's experimental results, however, are still low $3420 \text{ cm}^2/\text{Vs}$ [7]. The most notable event that restrict the mobility, which is produced at the interface during growth, is electron scattering at the charged dislocation centre [7]. So, increasing electron mobility could result from enhancing crystal quality by reducing dislocations [7].

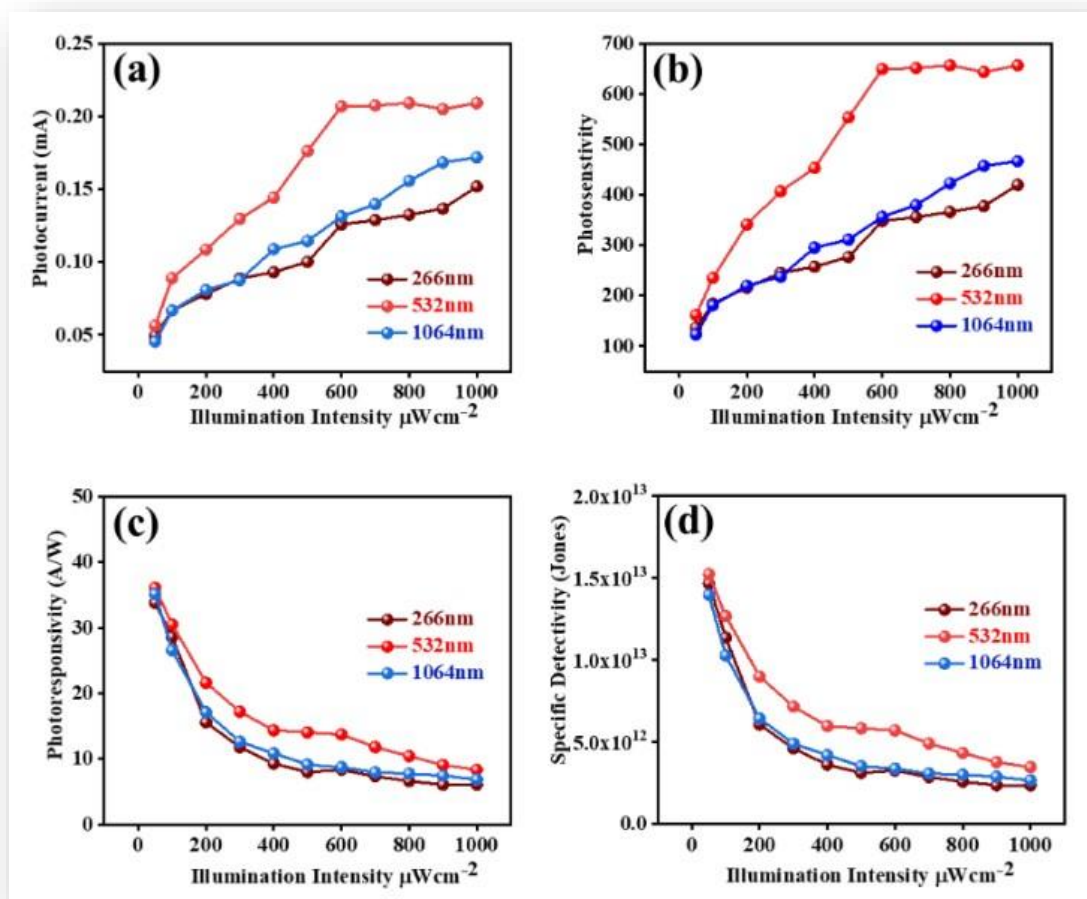


Figure 2.4 Illumination intensity-dependent (a) photocurrent, (b) photosensitivity, (c) photoresponsivity, and (d) specific detectivity of Ag/GaN/InN/Ag heterointerface photodetector under the illumination of 266 nm, 532 nm, and 1064 nm lasers. [7]

[Fig. 2.4](#) illustrates the photo-response vs. illumination intensity for varying illumination levels [7]. Ali Imran *et al.* states from [Fig. 2.4](#) that, the photocurrent and photosensitivity rise as the laser's illumination power rises [7]. Additionally, as the intensity of the illumination increases, the photoresponsivity and specific detectivity values fall [7].

2.1.6 Silicon Carbide (SiC)

A wide bandgap semiconductor with excellent properties, such as a high breakdown electric field (1.4 MV/cm), a high electron drift velocity ($2.7 \cdot 10^7$ cm/s), a high chemical stability in harsh environments, a high physical stability at high temperatures, a high thermal conductivity ($3.3\text{-}4.9 \text{ W}\cdot\text{cm}^{-1}\cdot\text{K}^{-1}$), and a high radiation resistance, is SiC [19]. SiC devices have become good prospects for micro-, nano-, and optoelectronic applications as a result of these outstanding characteristics and improvements in device fabrication [19]. SiC has a bandgap of 2.4 – 3.1 eV [14]. The high-speed operation of SiC device is the result of large electron saturation velocity of the compound semiconductor [14].

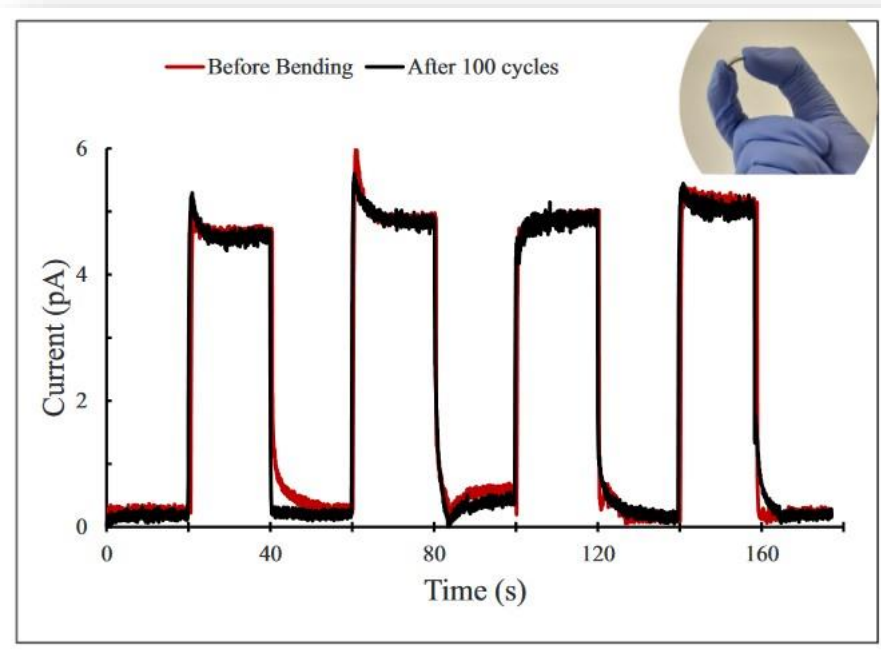


Figure 2.5 The photocurrent-time plots of the flexible SiCNW-UVPD before and after 100 bending cycles at 10 V bias voltage.[19]

Mustafa A. [Yildirim *et al.*](#), in the research “Self-powered fine-pattern flexible SiC single nanowire ultraviolet photodetector” depicts in the results in [Fig. 2.5](#) UVPD demonstrated exceptional electrical stability before and after 100 cycles of bending at 10 V, with only a very tiny decrease in photocurrent (less than 1%) after the bending test [19].

2.1.7 Zinc Oxide (ZnO)

In this paper the semiconductor for the UV radiation detection technology ZnO has been used for the Nano – sensor, which is the basic mechanism of the UV Monitor device. Research shows that ZnO are most eminent semiconductor candidate for UV radiation photodetectors [15,20]. ZnO has 3.37 eV and major exciton binding energy equal to 60 meV at room temperature [15]. Studies has reported high performance through different techniques of ZnO based films fabricated photodetectors such as p-n junction, p-i-n junction, Schottky junction etc which are more developed and improvised versions [20].

Nanowires (NWs), nanotubes (NTs), nanoparticles (NPs), nanobelts (NBs), Nanoflakes (NFs), quantum dots (QDs) and nanorods (NRs) different ZnO based nano materials have been utilized to improve the photo detection of the UV photodetector devices [21]. Nanomaterials unlike bulk and thin film counterparts shows more significant UV detection because of greater ratio of surface to volume [21]. In the UV photodetector device, the mechanism of photo detection is different from established methods. Established UV photodetectors are operated by external driving force such as voltage or current source [21]. From the viewpoint of device design and working principles. Conventional ZnO UV photodetector can be differentiate into three types, [Fig. 2.6](#), standard metal – semiconductor – metal (MSM) based UV photodetector, Schottky junction-based UV photodetectors and p – n junction (homo junction or hetero junction) based photo detectors.

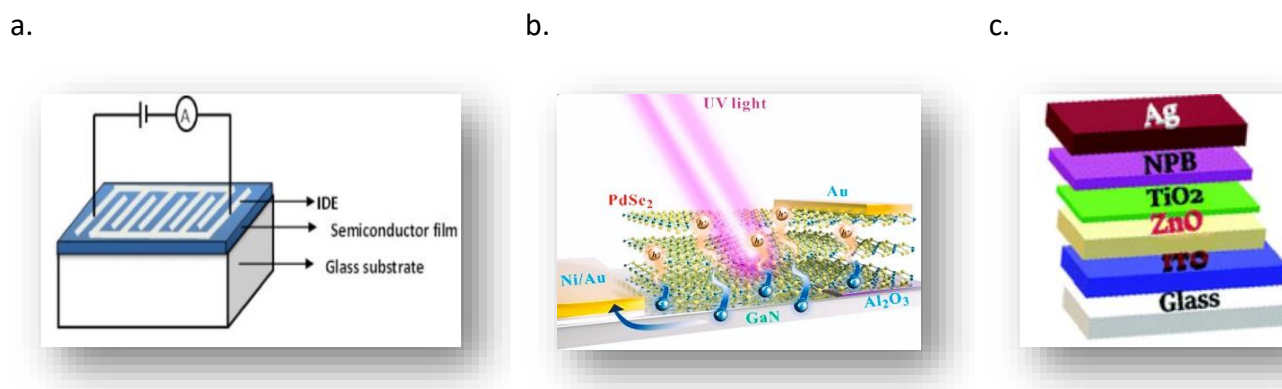


Figure 2.6 (a) Schematic of MSM photodetector [22], (b) Schematic of 2D palladium diselenide PdSe₂/GaN Schottky junction device [23], (c) Device Structure for ZnO thin films for p–n junction-based visible-blind ultraviolet photodetectors [24]

2.1.7.1 Conventional Zinc Oxide (ZnO) MSM based UV photodetector:

Pure ZnO nanomaterials with conventional MSM photodetector has been widely used for UV radiation detector for its simple fabrication process [21]. In the standard ZnO based photodetectors, a slow

photoresponsivity is noticed in the range of few seconds to minutes delay in the responsivity due to high resistivity, low charge carrier mobility and inherent defects. Research has been done for improving the photoresponsivity through increasing carrier mobility of ZnO based photodetectors by doping ZnO nano structures with other elements like hydrogen (H), fluorine (F), indium (In), aluminium (Al) etc [21]. The localized surface plasmon resonance (LSPR) has effect on nanomaterial which modifies their reaction to photoconduction by exciting electrons combining with ZnO when exposed to UV radiation [21]. Nanoparticles such as Au, Pt, Al, and Ag has been widely coupled with ZnO nanomaterials due to their prominent LSPR effect and thus increases photoconduction [21].

2.1.7.2 Schottky UV photodetector:

Schottky junction-based photodetectors has advantages of low dark current, high quantum efficiency, high UV visible contrast, viable zero bias operation, rapid switching operation and compliant photo conduction and response behaviour implying external driving force [28,29]. Among various Schottky barriers photodetectors, graphene and ZnO based Schottky barrier has gained significant attention because of intrinsic properties of graphene [21].

2.1.7.3 p – n junction-based UV photodetector:

It is a p – n junction photodiode which has been precisely fabricated to allow penetration of light in the proximity of the metallurgical junction [20]. The advantages of p – n and p – i – n junction photodiodes are speedy response, low dark current and operates without application of external biased [20]. These characteristics of p – n junction photodiode makes it more suitable for future of great technological advancement. In recent research studies the nature of homo and hetero junction of ZnO nano material-based UV photodetector has been mentioned for its built-in electric field generation at the interjection of the semiconductor to semiconductor which enhance the total photoconductivity through separating photo generative charges [20].

2.1.7.4 Homojunction photodiode:

It is known that involuntarily doped ZnO is commonly n – type semiconductor because of the intrinsic defects (i.e., oxygen voids) [20]. Consistent method to produce p – type ZnO film which is important for fabrication of p – n junction is even appealing for several reasons like self – compensation process, deep acceptor levels and low solubility of the dopants [20]. Researchers have fabricated different types of homojunction ZnO based photodetectors which are, ZnO:(Ag,N)/ZnO NRs p–n homojunction, CdMoO₄-ZnO composite film, p-Mg_{0.2}Zn_{0.8}O/n-ZnO homojunction, vertically stacked ZnO sheet-like nanorod p–n homojunction, p–n ZnO NW homojunction and many more [21].

2.1.7.5 Heterojunction photodiode:

Due to the disadvantages of the homojunction photodiodes mentioned above, heterojunction photodiodes are used to fabricate ZnO based UV photodetector with different types of p – type semiconductors, for example SiC, Si, GaN and some more, where the silicon fabrication with ZnO photodetector has been commercially adapted because of low cost and broadly used integrated circuit technology [20]. Different research studies on heterojunction ZnO based photodetector are, ZnO/Si heterojunction, p-GaN/n-ZnO NRs heterojunction, ZnO NP-graphene core–shell heterostructure, ZnO NR/graphene heterostructure and many more [21].

Recently nano – structuring of wide bandgap semiconductors has proven successful than conventional technologies. The development of such technology has proven low cost, durable in severe condition, and high-quality photo sensitivity. Researchers are investing further studies behind the development of the wide bandgap semiconductors for improving the photo responsivity, photo detection, conduction, gain and other prominent factors to be more precise and accurately reliable. Nano – structure dimensions for the wide bandgap semiconductors are also investigated at a great demand. Practical implementation and successful photo detection devices has been constructed with different semiconductors like ZnO, GaN, TiO₂ etc.

Among the application of different wide bandgap semiconductors, ZnO has got renowned reputation for its durability in all condition, easy fabrication, constant bandgap of 3.37 eV at room temperature and high sensitivity to visible lights. Instead of being so famous semiconductor for photo detector devices, ZnO photo responsivity is still on the research process for further prominent nature of the semiconductor. Despite of various merits of the semiconductors there is still plenty of room left for development. Along with their use in photo detector devices, there are other applications which can use their advantages for fast response.

2.2 Fabrication Technology

Nano fabrication is generally divided into two process top – down nano fabrication and bottom – up nano fabrication [26]. In the top – down nano fabrication processes the materials are broken down into smaller structure until the desired structure is achieved [25]. In the bottom – up nano fabrication processes the atomic or molecular structures are build up in a desired structure [25]. Top – down nano fabrication is good for long range order and ensuring macroscopic connection whereas, bottom – up nano fabrication is better for short range order at a nano scale dimension [25]. The integration of the both the process in a one product results in the best structure integrity in a device.

The industrial nano fabrication process comprises the combination of both processes and can be categorized further into three more sub processes of nano fabrication which are thin film deposition, lithographic patterning and physical or chemical etching [26].

2.2.1 Thin film deposition:

Thin film nanofabrication technique is the layers of polymers, metals, semiconductors etc with nanometre level of thickness, where these materials are fabricated using various deposition process of atomic layer deposition (ALD) [27], molecular beam epitaxy (MBE) [27], chemical vapour deposition (CVD) [27], pulsed laser deposition (PLD) [27], radio frequency (RF) magnetron sputtering [27], and flame spray pyrolysis (FSP). Among them, FSP is one of the efficient techniques to fabricate thin layer of metal oxide films including ZnO, TiO₂, and SnO₂, to name a few. Using this technique, a thin film is deposited by spraying a solution on a heated surface and the constituent's reaction results in the formation of chemical compounds. In FSP synthesis technique, the evolution of metal oxide nanoparticles depends on a variety of droplet (liquid) and vapour phase-related physical mechanisms, such as precursor evaporation, oxidation, nucleation via a gas-to-particle conversion mechanism, and subsequent particle (solid) growth mechanisms based on coagulation, sintering/coalescence, and agglomeration [27].

Research has shown that from past two decades, FSP has proven a propitious technology in both the laboratory and industrial level for accelerated single step synthesis of single or combine element nanoparticles. A highly promising and adaptable method for the quick and scalable synthesis of nano structural materials with tailored functions is the combustion of suitable precursor sprays in a FSP process. The basic principles of the long-used vapour-fed flame aerosol reactors, which were widely used for producing commonplace powders such as pigmentary titania, fumed silica, alumina, and even optical fibres, were the source of the original technology. The application of the nanoparticles in the FSP technique conquers in numerous implementation such as nano sensors, batteries, food fortification, biomaterials, and many more [27]. Flexible designs of nanostructured loosely aggregated powders and particulate films of pure or mixed oxides, and even pure metals and alloys, have been made possible by significant advancements in FSP reactor engineering and precursor chemistry. With the help of this essentially one-step, continuous FSP process, novel material morphologies like core-shell structures and nanorods are made possible [28]. The very easy synthesis and provision of the combustible liquid precursor-solvent mixture, in which almost all elements of the periodic table may be considered in various combinations with one another, is a major factor in the FSP's tremendous success. On the contrary, the manufacture of single-oxide nanoparticles is more constrained by the lack of enough supply and the more difficult handling of acceptable gaseous precursors in vapor-fed flame reactors. In the FSP technique, a flammable carrier solution that is atomized and dispersed with oxygen into a spray of tiny droplets contains a metal-containing precursor that

has been dissolved in it. A pilot flame's released enthalpy permits spray ignition, droplet evaporation, and precursor conversion. If particle nucleation and growth take place after precursor evaporation such as gas-to-particle conversion and inside the liquid droplet depends heavily on the liquid and gaseous thermo-physicochemical characteristics and chemical nature of the educts at high temperatures such as droplet to particle conversion. In the [Fig. 2.7](#) below nanoparticles evolution in FSP technique has been shown.

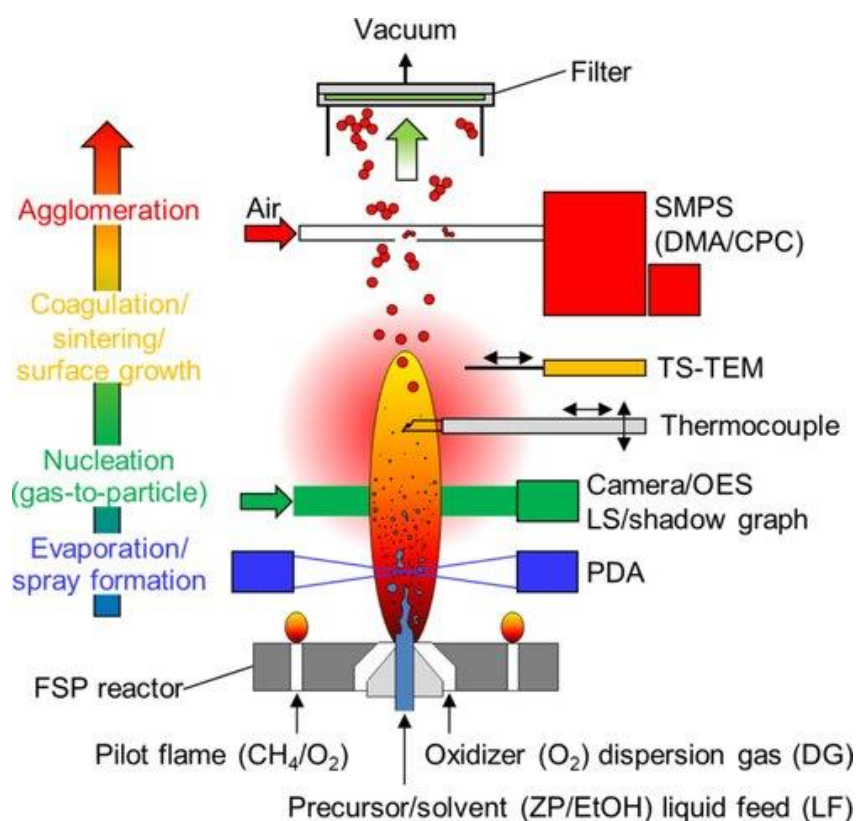


Figure 2.7 Nanoparticles evolution in FSP technique [27]

2.2.2 Lithography:

The lithography nano fabrication process includes the patterning of the deposited thin films into integrated circuit structural system and at last the etching process is finalised by the finalizing the desired operational section of the materials and removing the unnecessary part [29]. There are several different types of lithography, including photolithography, electron beam lithography, X-ray and extreme UV lithography, focused ion beam and neutral atomic beam lithography, soft lithography, colloidal lithography, nanoimprint lithography, scanning probe lithography, atomic force microscope nanolithography, and others [30]. Electron beam lithography is the nanofabrication technique where devices are created at a nano scale level materials through utilizing electron beam to scan the material and formation of the required structure. Magnetic lenses are used for focusing the electron beam on the materials [29]. The general use of the electron sources are the thermionic emitters and the thermal field emitters with an output range of 1 to 200

KeV but 50 to 100 KeV range is used for the fabrication process. Researchers have demonstrated resolutions under less than 10 nm in this fabrication technique [29]. The disadvantage of this technique is the higher purchase cost and high maintenance issue [29]. The focused ion lithography technique uses ions instead of electrons for resisting a pattern. The ions are produced from the liquid metallic tip with elements like gallium, through filtration of one type of ions to induce with resist pattern focusing on the surface through electrostatic lenses [29]. The operational energy of this method is 10 to 200 KeV. The focused ion beam lithography can go to the range of 20 nm with 5 nm lateral feature size [29]. The disadvantages of this method is the comparative speed of ions due to lower ion current density opposite of the electron in electron ion beam lithography method.

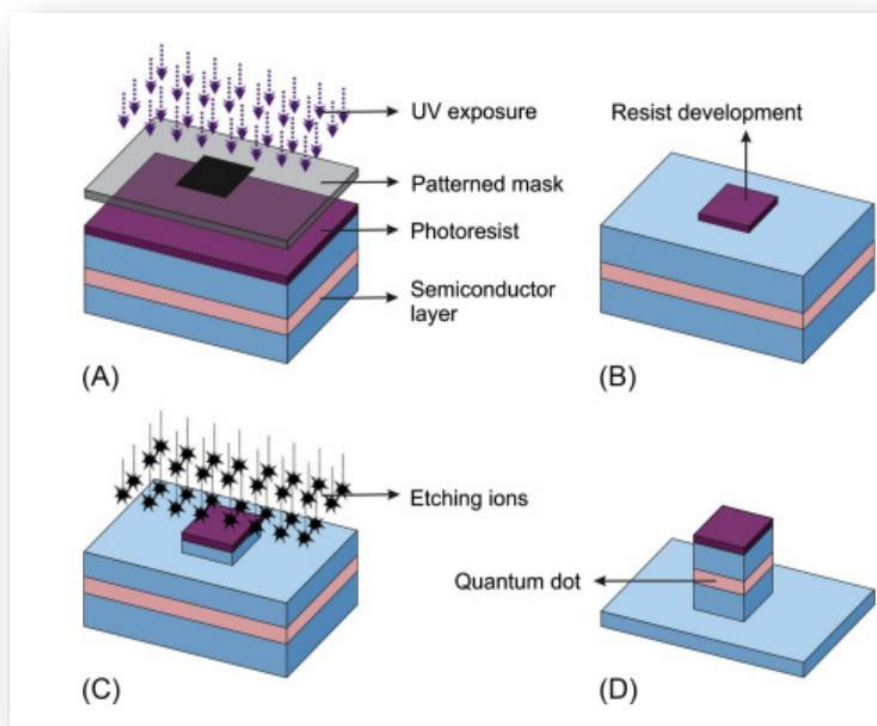


Figure 2.8 Photolithography Process [30]

2.2.3 Physical and Chemical Etching:

Etching is a technique that removes material off a surface selectively using physical or chemical processes in order to produce topographical features [29]. Etching can be anisotropic if it moves in a certain direction or isotropic if it moves evenly in all directions [29]. Liquid chemicals or gaseous physico-chemical reactions are utilised in the mechanisms for etching [29]. Wet etching and dry etching are the more popular names for these two techniques [29]. Wet etching is a procedure that uses a chemical liquid that is either acidic or basic to process the material and remove undesired material from a surface [31]. In a vacuum environment, dry etching process changes gas into plasma [31]. Although the term "dry etching" is

sometimes used interchangeably with "plasma etching," it also refers to etching processes that don't involve vacuum or Radio Frequency (RF) fields [31].

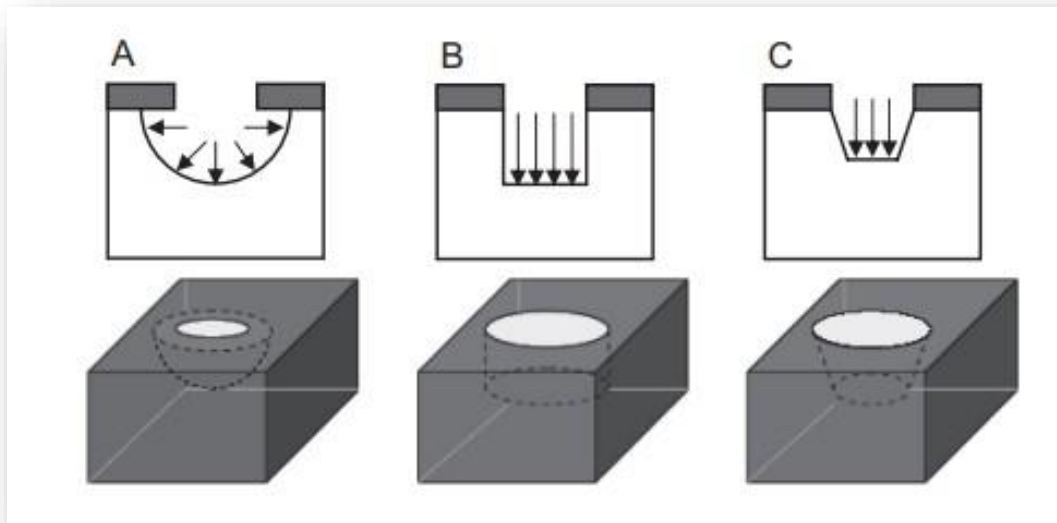


Figure 2.9 Etching profiles generated with (a) isotropic etching, (b) dry anisotropic etching, and (c) wet anisotropic etching [29].

Among the various fabrication process, FSP has been used for fabrication of the UV nano sensor for this project. The details of the fabrication of this UV nano sensor will be describe in the next chapter.

Chapter Three

Materials, Devices and Methods

Chapter 3 – Materials, Devices and Methods

In this paper, for the development of UV nano sensor, ZnO nanoparticle aerosols were created and directly deposited onto glass substrates with a series of interdigitated electrodes using a FSP (FSP) technique.

3.1 Materials

The materials used for the fabrication of the nano sensor are, Zinc naphthenate and xylene. The following is how the photodetector nanoparticles were created: Xylene (Sigma Aldrich) was used to dilute Zinc Naphthenate (10% Zn, Strem Chemicals), which had a total metal atom content of 0.3 mol L⁻¹ for Zn. A syringe pump was used to deliver the prepared solution at a rate of 5 mL/min while dispersing it into a thin spray with 5 L/min of oxygen at a continuous pressure drop of 2 bars.

3.2 Mechanism, Apparatus, contents

Thin-film technologies are used to create metal-based InterDigitated Electrodes (IDE) on a glass substrate by micrux technologies, [Fig. 3.1\(b\)](#). The interdigitated electrodes offer a useful tool, especially for fuel cells and impedance, capacitance, and conductivity studies. Thin-film technology allow for the precise and high-resolution manufacturing of microelectrodes (<25 μm). Thin-film interdigitated electrodes are an effective tool for improving analytical parameters in a variety of applications by utilising their inherent qualities, such as low cost and disposable nature, reusability, high fabrication resolution, high sensitivity, low reagent consumption, and ease of pre-cleaning. Two individually programmable microelectrode array strips made using an interdigitated technique make up the simplest interdigitated electrodes (IDE). There are no extra reference electrodes or auxiliary electrodes on the apparatus. Different widths and spacing are available for Interdigitated Electrode (IDE) designs in platinum or gold. For this sensor, reference no -ED-IDE3-Pt, material - Ti/Pt, μElectrode width of 5 μm, μElectrode gap of 5 μm, number of feet - 180 pairs and thickness of 50/150 nm substrate has been used. In numerous analytical applications, interdigitated electrodes (IDE) can be employed with electrochemical impedance spectroscopy (EIS), a potent, quick, and accurate non-destructive technique.

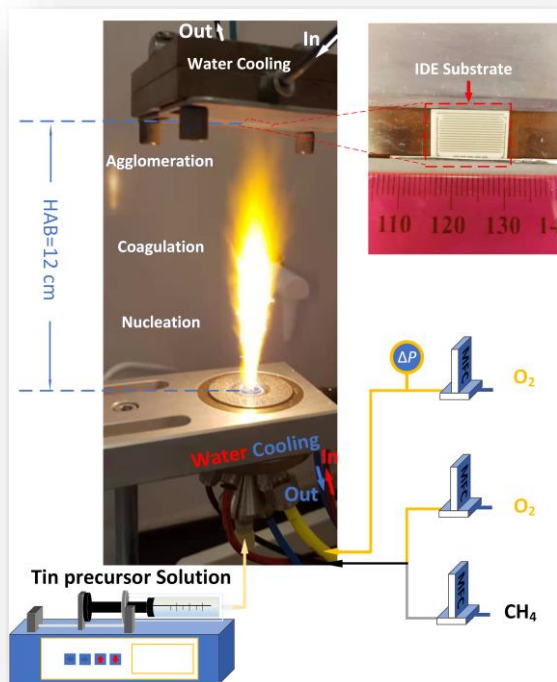
3.3 Method

UV Photodetector Fabrication:

In [Fig. 3.1 a](#), the spray was ignited by supporting premixed methane/oxygen flames (CH₄ = 1.25 L·min⁻¹, O₂ = 1.3 L·min⁻¹). A water-cooled substrate holder placed at 12 cm height above the burner (HAB) was

utilized to keep the substrate temperature below 220 °C. The photodetector substrates were made of glass with interdigitated platinum lines with 5 μm width and spacing and an active circular area of 3.5 mm in diameter (ED-IDE2-Pt, Micrux Technologies). The prepared thin films were annealed (Compact muffle/tube 2-in-1 furnace, Zhengzhou TCH) at 300 °C for 12 hours at ambient pressure.

a.



b.

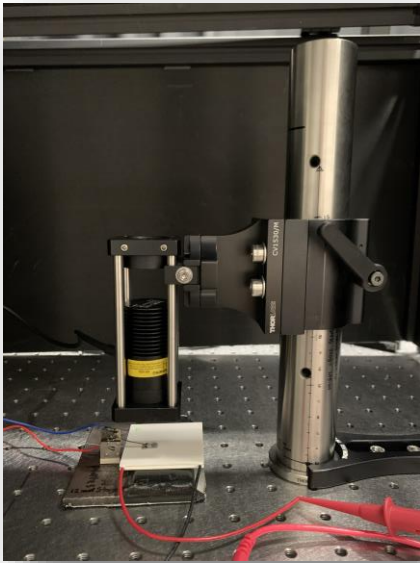


Figure 3.1 (a) FSP Fabrication process, and (b) Thin-film Platinum InterDigitated Electrode (5/5 μm) [32]

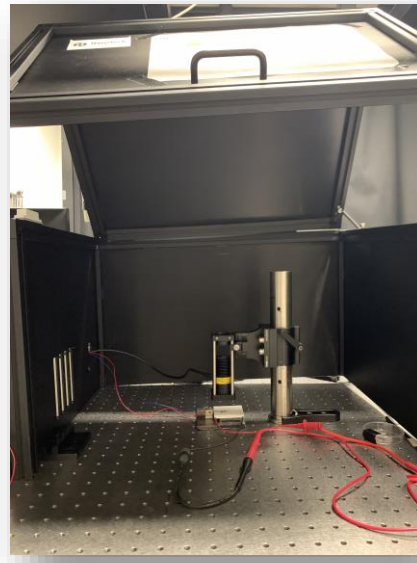
3.4 Sensor Testing Apparatus

The sensor has been tested under Thorlabs light setup and the device has been tested in the Thorlabs laboratory box setup. In [Fig. 3.2](#) the indoor laboratory UV light setup along with the source meter and light controller has been demonstrated.

a.



b.



c.



d.



Figure 3.2 (a) Thorlabs Laboratory modular optical tweezer setup, (b) Black box light setup, (c) DC2200 - High-Power 1-Channel LED Driver with Pulse Modulation, 10.0 A Max, 50.0 V Max [33] and (d) Keithley 2450 – Source Meter Instrument (200 V, 1 A, 20 W) [33]

The [Fig. 3.2](#) provides the testing procedure of the UV nano sensor under light setup in the laboratory. The setup is compacted under a boxed walls all around the setup so that the UV light cannot reach out of the box during experiment for safety protocol. The sensor as shown in [Fig. 3.2\(a\)](#) is placed under UV light diode of 375 nm which has been used for this project. The sensor has been placed on a raised bar to avoid contact with the table. For the UV light 375nm has been chosen for the wavelength falling under UVA radiation (315nm -400nm). The sensor then provided in contact with two needles for connection with the 2450 source meter and the UV diode is controlled by LED driver. The LED driver controls the current of the LED. For this project the LED controller is varied along 20 mA, 40mA, 80 mA and 150 mA. The sensitivity of the sensor is tested through a software in the computer connected with the source meter. The

source meter provides voltage across the sensor and current is passed through the internal circuit of the setup. The source meter is made to provide 3.3V. The sensitivity of the sensor is then tested by determining the resistance change of the sensor during the LED is turned OFF and ON turning rotationally. The resistance of the sensor drops when the LED is turned ON and the sensor sense the presents of the UV light and passes the current across it. The resistance goes high when the LED is turned OFF and the sensor blocks the current across it. **The current density of the LED driver has been provided in 3.1.**

Table 3.1 – LED current and Light Density

Current (mA)	Power (mW)	Diameter(cm)	Radius(cm)	Area(cm ²)	Light Density (mW/cm ²)
0	0.009	1	0.5	0.7854	0.011459129
20	0.239	1	0.5	0.7854	0.30430354
40	0.515	1	0.5	0.7854	0.655716832
80	1.093	1	0.5	0.7854	1.391647568
150	2.15	1	0.5	0.7854	2.73745862

The sensor has been tested under different condition of temperature. The sensor testing results along with sensor performance is reported in Chapter 5 – results and discussion.

Chapter Four

UV Sensor System

Chapter 4 – UV Sensor System

The UV index monitoring device has been designed in the basis of ohm meter circuit with Arduino microcontroller. The component has been selected on the basis of design structure and desired functionality of the device. In this chapter, the design electrical components, connections and mobile application will be discussed in detail.

4.1. Electronic components

[Table 4.1](#) contains the list of main electronic components and their functions utilised for the UV sensor system.

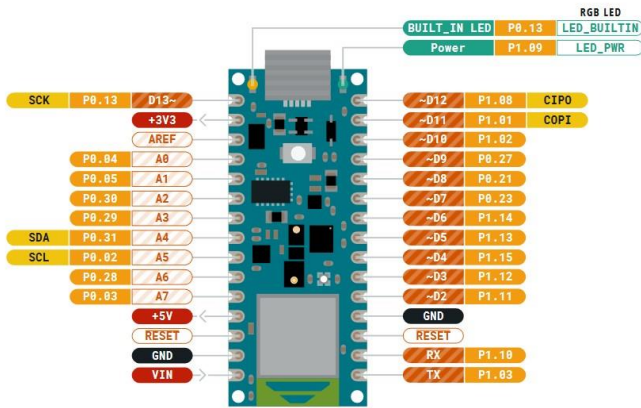
[Table 4.1](#) – Electronic Components used in the UV sensor system

Components	Functions
1. Arduino Nano 33 BLE Sense	This is the controller used for the system. Arduino reads the UV sensor data; calibrates it with using stored look-up tables; passes it on to the mobile app via Bluetooth.
2. Resistor	A known resistor of value 220 Ω is used in a voltage divider circuit to evaluate the UV sensor resistance.
3. Polymer Lithium Ion Battery (LiPo)	3.7 Volt 120 mAh LiPo rechargeable battery is used for powering the circuit through Arduino nano 33 BLE sense.
4. Adafruit Micro Lipo w/MicroUSB Jack - USB LiIon/LiPoly charger - v1	The MicroUSB charger is used for charging the Lipo battery.
5. Single Pole Double Throw (SPDT) slide switch	The switch will function for the device to be either in charging mode or operation mode.
6. Vivo android version 12 smartphone	This phone hosts the app and connect to the UV sensor device through Bluetooth for data acquisition.

The components in the above [Table 4.1](#) are described with their respective characteristics and performances in the below sections:

4.1.1 Arduino Nano 33 BLE Sense:

a.



b.

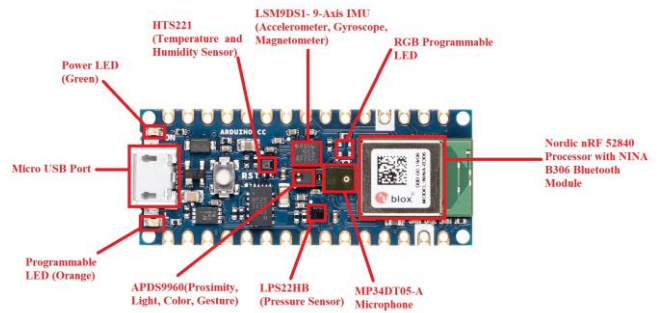


Figure 4.1 (a) Arduino Nano 33 BLE Sense pinout diagram and (b) different sensor on the board. [34]

The Nordic Semiconductors nRF52840, a 32-bit ARM® Cortex®-M4 CPU operating at 64 MHz, is the processor used in the Arduino Nano 33 BLE Sense, a development of the original Arduino Nano [34]. This version of Arduino nano has been selected on the basis of its specification mentioned in [Table 4.2](#) below.

[Table 4.2](#) – Technical Specification of Arduino Nano 33 BLE Sense [34]

Features	Specification
Microcontroller	nRF52840
Operating Voltage	3.3V
Input Voltage (limit)	21V
DC Current per I/O Pin	15 mA
Clock Speed	64MHz
CPU Flash Memory	1MB (nRF52840)
SRAM	256KB (nRF52840)
EEPROM	none
Digital Input / Output Pins	14
PWM Pins	all digital pins
UART	1
SPI	1
I2C	1
Bluetooth®	NINA-B306

The Arduino Nano 33 BLE sense not only is a very well form microcontroller board with splendid technical specifications but also number of embedded sensors are included in this board in [Fig. 4.1](#). The sensors are:

1. This board is perfect for wearable technology because of its 9-axis inertial sensor.
2. Temperature and humidity sensors are used to provide extremely precise measurements of the environmental conditions.
3. A barometric sensor can be used to create a basic weather station.
4. Microphone: for real-time sound recording and analysis.
5. Sensors for gesture, proximity, light colour, and intensity help determine whether someone is moving close to the board while estimating the brightness of the space.

All this sensor in the board makes it more technology perfect for developing different possible devices for wearable engineering. The ability to run Edge Computing applications (AI) utilising TinyML is the key feature of this board, in addition to the remarkable array of sensors [34]. The Nano 33 BLE Sense's communications chipset supports Bluetooth® Low Energy and Bluetooth® client and host devices [34].

The purpose of selecting Nano 33 BLE sense is the primary feature of having Bluetooth low energy in the same microcontroller chip and the Bluetooth low energy makes the device more power sufficient. BLE is a type of wireless communication made specifically for short-range communication. All BLE devices use 40 channels scattered throughout the 2.4GHz band to operate [35]. Because it transmits short data packets and creates connections quickly, it supports multiple connections running concurrently [35]. On the hand, traditional Bluetooth can only start 7 connections at once [35]. The practical range varies between 30 metres, a transmitter at 0.01mW and receiver with -70dBm sensitivity to 100 metres depending on the transmission power/reception sensitivity i.e., Tx at 10mW and Rx -90dBm. Up to 20 connections can be established simultaneously through BLE [35]. The current consumption for this device under no UV Radiation is around 22.22 mA and during sleep mode it is 18.89mA. Under intensity of UV radiation, the highest current consumption for the device reaches around 37 mA to 45 mA. The nano provides great range of opportunities for this project. It not only communicates through Bluetooth but with different sensors present in its chipset makes it possible for more scope for the project. The project as mentioned earlier has the target of achieving a well-equipped functional wearable device. For the device to be wearable, the technology developing the device needs to be more precise in structure for overall device dimension and weight. The selection of nano 33 BLE sense not only makes the device smart in communication but also makes it possible weight for wearable device which can be wear or mount on the body and the user can carry it everywhere. BLE is designed for applications where long battery life is more important than fast data transfer rates.

4.1.2 Resistor:

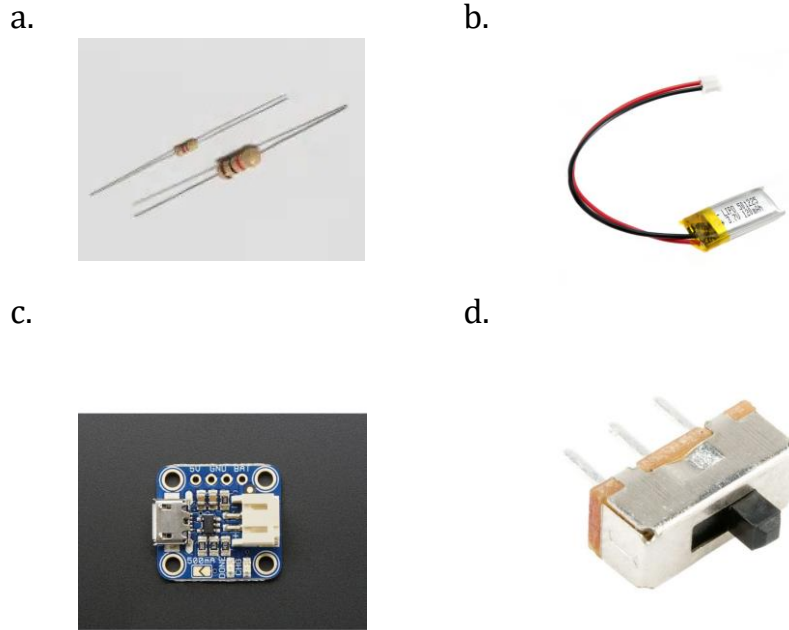


Figure 4.2 (a) Resistor [36], (b) Lipo battery [37], (c) Adafruit Micro Lipo w/MicroUSB Jack - USB LiIon/LiPoly charger - v1[38] and (d) SPDT slide switch [39]

The UV index is calculated from the UV-dependent conductivity (or resistivity) of the nano sensor. The voltage across the nano-sensor is measured and the unknown resistance is calculated with respect to the known resistance. The ohm meter circuit constructed with Arduino measure the voltage drop and resistance of the unknown component by applying voltage divider formula in the circuit. In this project 220-ohm resistor has been used to pass the current in the circuit and hence to obtain appropriate values from the sensor.

4.1.3 Polymer Lithium Ion Battery (LiPo):

A 3.7 V 120mAh rechargeable LiPo battery powers the system. in [Fig. 4.2 \(b\)](#). The battery dimension is 28x13x5mm and 11 gram in weight [36]. The other features of the battery are, 2C continuous discharge, great energy retention with low self-discharge rates with less than 8% per month and reliability under extreme conditions within a temperature range of -10°C to 50°C [36].

4.1.4 Adafruit Micro Lipo w/MicroUSB Jack - USB LiIon/LiPoly charger - v1:

The Lipo battery ([Fig. 4.2 c](#)) is provided with a charger port in the circuit, which will make the battery recharged as it requires and thus makes the device more compatible to operate along the day. The charger has 5V input via Micro-B USB connector [38]. It is eligible for charging single Lithium Ion/Lithium Polymer 3.7/4.2v batteries [38]. By default, the charging current is 100mA [38]. A preconditioning charge, a fast charge at a constant current, and a trickle charge at a constant voltage are the three stages of charging that are used to maintain the battery full [38]. When the charger is connected to a power source using its MicroUSB connector, the LED on the charger will flash to indicate that a battery is not present; it will remain on while charging and turn off once the battery is fully charged.

4.1.5 SPDT slide switch:

The SPDT slide switch shown in [Fig. 4.2 \(d\)](#), has been used for switching the mode of the device from operation to charging. The device will be charger if the switch is slide to the connection towards the charger and the device will remain active if the switch is being slide to the power mode. The switch makes it easy for the device to indicate the state of the device it is sided to.

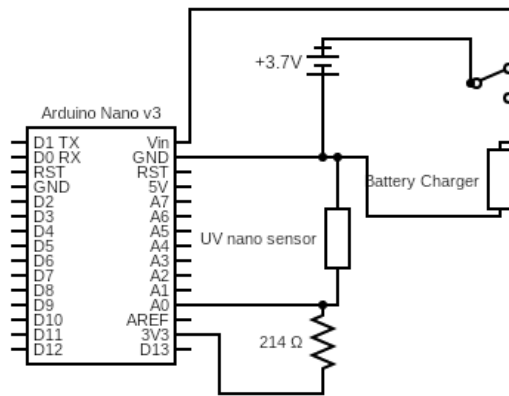
4.1.6 Vivo Android 12 smartphone:

VIVO Y11s Dual Sim smartphone has been used for this project. The android smartphone makes it easier for mobile application for any projects easier through android operating system. It is easier for primary mobile application development in android platform other than iOS operating system.

4.2 Device Design

This section of the chapter will describe the circuit design and working principle of the device. The UV index monitoring device as mentioned in this chapter above is developed according to the basic ohm – meter circuit design. In [Fig. 4.3](#), the circuit diagram and the final device structure has been shown.

a.



b.

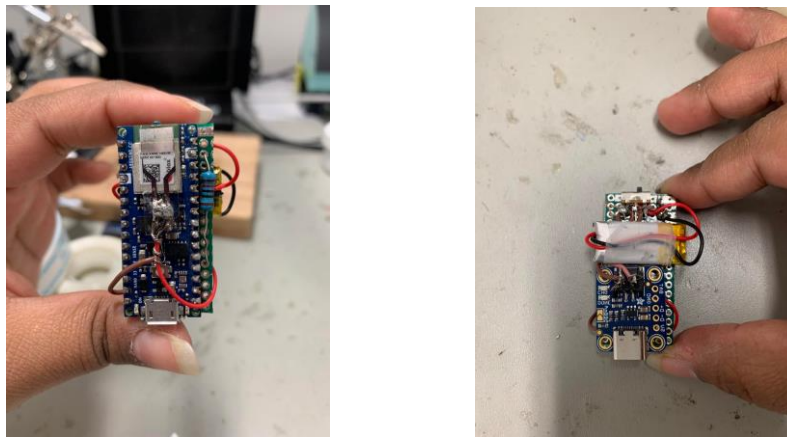


Figure 4.3 (a) UV index monitor device circuit and, (b) practical implementation of the circuit in a compact device structure.

In the [Fig. 4.4](#), R_1 is the known resistor of value 220 ohm, R_2 is the UV nano sensor (resistivity across the sensor is measured for determining UV radiation), V_{out} is the Analog (A_0) pin of the Arduino, V_{in} in the input of the Arduino and GND is the common ground. The UV nano sensor (R_2) is connected with the GND pin of the Arduino in one end and the other end is connected in series with the R_1 known value resistor at A_0 pin of the Arduino. The Arduino is powered by 3.7 V battery connected to the SPDT switch 1 and the negative wire of the battery is connected to the GND pin of the board. The Battery charger positive wire is connected to the SPDT switch 2 and the negative with the GND pin. The SPDT switch 1 toggle between battery and the charger. The switch 1 connects with switch 2 to power the device through battery and the switch 1 connects with switch 3 to connect the charger with the battery for charging mode. The device does not operate in charging mode and vice versa.

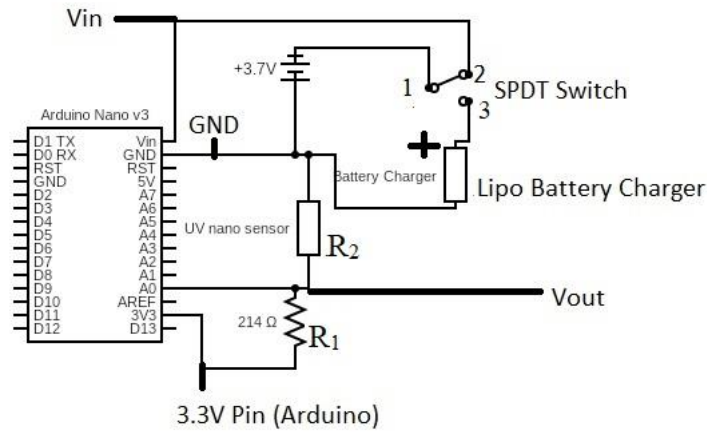


Figure 4.4 UV index monitor device connection diagram

The below theoretical calculation for unknown resistor values i.e., the resistance across the sensor has been carried out in the Arduino IDE for calibrating the results.

The ohm law equation,

$$V = I \times R \dots\dots \text{equation (1)}$$

where V is the voltage, I is the current and R is the resistance.

For resistor is series connection the formula –

$$V = I \times (R + R_n) \dots\dots \text{equation (2)}$$

where V is the voltage, I is the current and R is the resistance and R_n is the number of resistors added in series within the circuit.

For determining resistance of only one resistor in the circuit with multiple resistors is series connection, Voltage divider formula is followed –

$$V_{out} = V_{in} \times \frac{R_2}{R_1 + R_2} \dots\dots\dots \text{equation (3)}$$

Here, V_{out} is the voltage across the sensor, V_{in} is the 3.3v from the Arduino or power source, R_1 is the known resistor and R_2 is the resistance of the sensor.

For determining the resistance of the sensor (R_2) in equation 3 –

$$V_{out} = V_{in} \times \frac{R_2}{R_1 + R_2}$$

multiplying both side by $R_1 + R_2$

$$\gg V_{out} \times R_1 + V_{out} \times R_2 = V_{in} \times R_2$$

$$\gg V_{in} \times R_2 - V_{out} \times R_2 = V_{out} \times R_1$$

taking the R_2 variables in one side

$$\gg R_2 \times (V_{in} - V_{out}) = V_{out} \times R_1$$

taking the R_2 common

$$\therefore R_2 = \frac{V_{out} \times R_1}{V_{in} - V_{out}} \dots\dots \text{equation (4)}$$

Hence the resistance of the sensor can be obtained from equation 4 and thus it depends on the known resistor R_1 , input voltage V_{in} and output voltage V_{out} .

4.3 Mobile Application

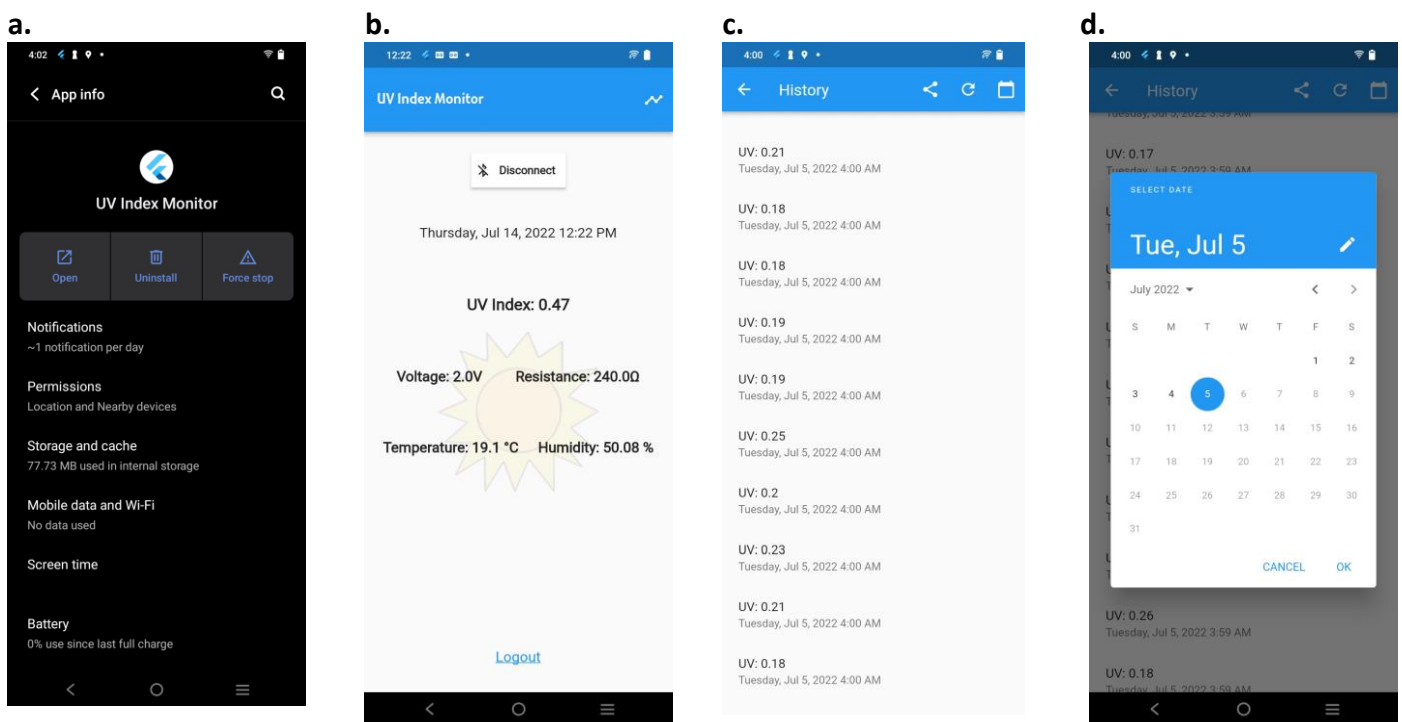


Figure 4.5 (a) UV Index Monitor mobile application, (b) UV index monitor user interface, (c) Application data history and (d) calendar chart for the data

As shown in [Fig. 4.5](#), the mobile application has a multi- page user interface. The user interface indicates the real time date, time, and day. The application indicates the data history page and store the data within the application. The application data history appears date wise with a calendar date format. The application has data sharing option which allows the application to share the data with other platforms. The data can

be refreshed from time to time. the user can terminate the connection from disconnecting the application from the device anytime. The application allows the users to create their individual profile and hence the data collection of the application is basically stored with specific user profile.

The app was created using Flutter SDK. The mobile application is created by Flutter using the C++-like Dart language. Android Studio has been used as the IDE, and Dart and Plugin have been installed. Data storing software for the mobile application has been implemented using Google Firebase. User registrations and application data are stored in Firebase's Cloud Fire Store Database.

Chapter Five

Results and Discussions

Chapter 5 – Results and Discussions

This chapter presents the test procedures and the performance results from the UV nano sensor and the UV index monitor. These tests were performed both indoors and outdoors. The indoor tests were conducted under Thorlabs Laboratory modular optical tweezer setup, varying different LED current ([Table 3.1](#)); the outdoor tests were conducted under direct sunlight at different times and conditions of the day.

5.1 Sensor Testing Results

The sensor has been tested under 4 different LED current (Table 3.1) and across 4 different temperatures (25°C, 30 °C, 35 °C and 40 °C). The temperature effect on the sensor and its performance evaluation has been carried out.

For changing the temperature in the laboratory setup, mcte1-199131-s peltier module, 200w, 50 x 50 x 3.5mm has been used to obtain different specific temperature for the sensor testing ([Fig. 5.1](#)).

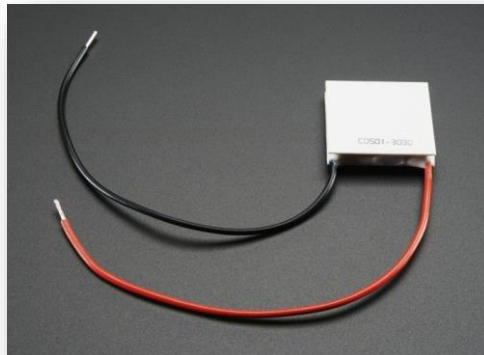


Figure 5.1 mcte1-199131-s peltier module, 200w, 50 ×50 ×3.5mm [40]

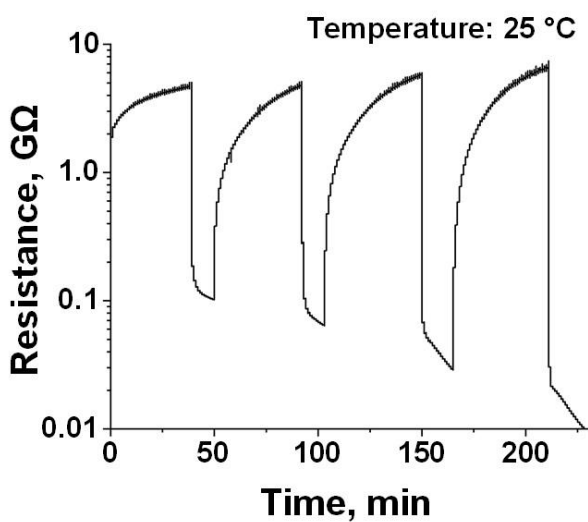
The peltier module has been connected under the sensor and through DC power source the module has been supplied continuous power till it reaches certain destined temperature. The module has been calibrated through testing by providing certain voltage and current to observe the rising of the temperature to desired level and the stability of the desired temperature and the reaction of the sensor at those specific temperature [Table 5.1](#). The temperature varies along the time as the module get heated and thus the desired temperature is respectively closed to the temperature obtained.

[Table 5.1](#) – Peltier Module Temperature calibration chart

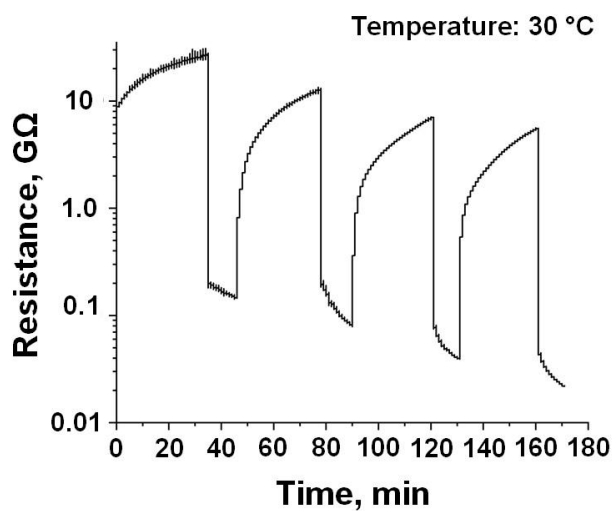
Voltage (V)	Current (A)	Obtained Temperature (C)	Required Temperature (C)
1.33 V	0.464	26 degrees	25 degrees
2.33 V	0.787	31 degrees	30 degrees
2.33 V	0.784	35 degrees	35 degrees
3.33 V	1.086	41 degrees	40 degrees

The [Fig. 5.2](#) will provide the performance of the sensor under different LED current and different Temperature.

a.



b.



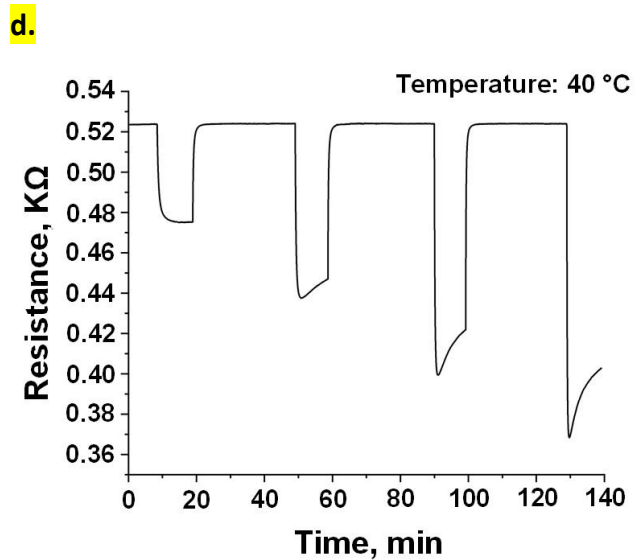
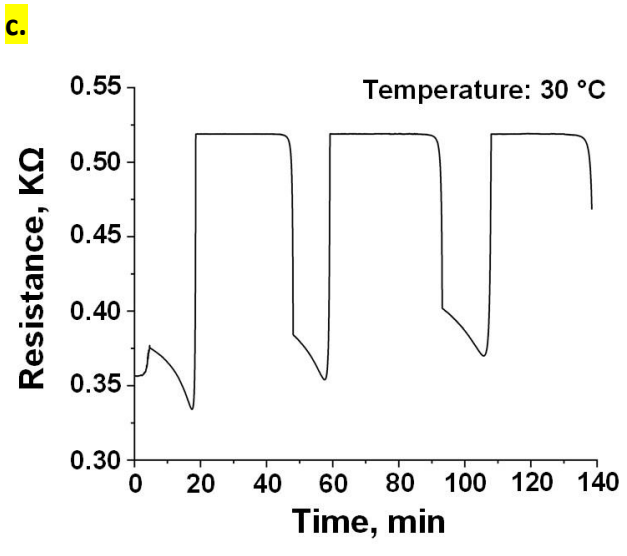


Figure 5.2 Resistance versus Time graphs at different temperature of (a) 25°C, (b) 30°C, (c) 35°C and (d) 40°C, at the light density of 20mA, 40mA,80mA and 150mA, respectively.

The UV nano sensor has been tested under four different LED current of the laser diode of 375 nm wavelength, 20mA, 40mA,80mA and 150mA, respectively at four different constant temperature of 25°C, 30°C, 35°C and 40 °C respectively. The dark current test was confined in the black box setup in the laboratory. The [Fig. 5.2](#) depicts the resistivity effect of the sensor when exposed under 4 different density of LED current. [In the Fig. 5.2 a & b](#), the resistivity of the sensor under 20mA, 40mA,80mA and 150mA LED current demonstrate standard behaviour of passing current through the sensor and acquiring lowest value of resistance. The sensor [in Fig. 5.2 a & b](#), when not exposed to dark current from the LED achieves Giga-ohm (GΩ) range of resistance and under the dark current lowers down to Mega-Ohm (MΩ) range of resistance. The effect of rising temperature on the sensor is demonstrated in [the Fig. 5.2 c & d](#), depicts the change of resistivity of the sensor, which lowers down from GΩ to Kilo-Ohm (kΩ) range of resistance and thus it indicates the effect of increase temperature on the sensor at higher temperature. The resistivity of the sensor changes due to the increase of the temperature, which makes the sensor absorbed the high temperature and sets the resistivity of the sensor in the lower range.

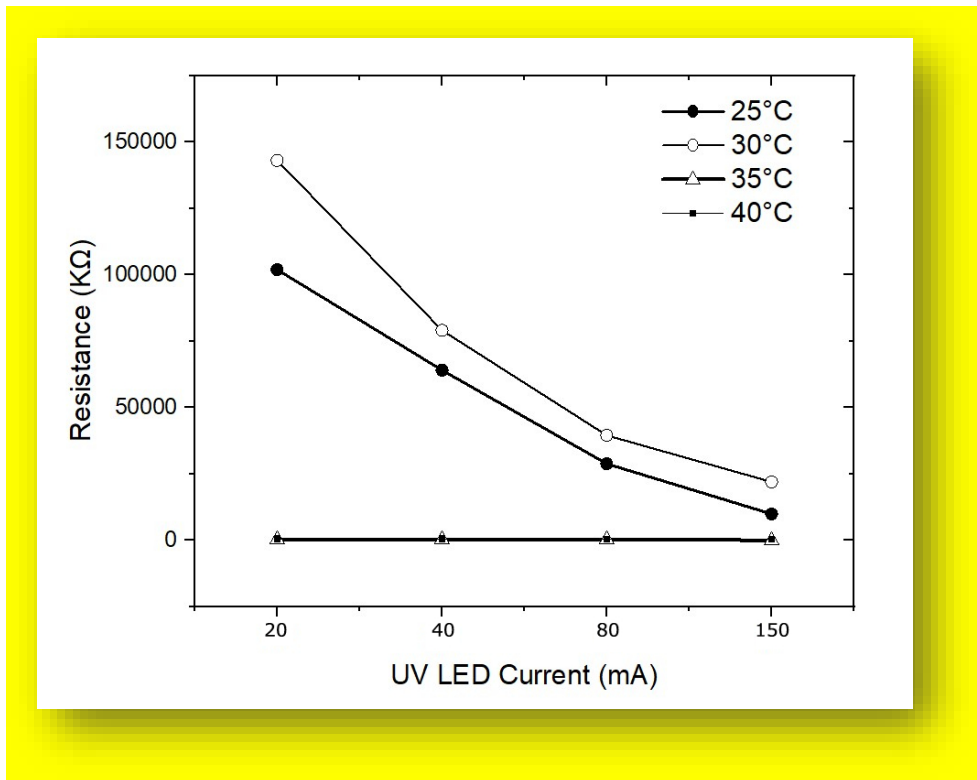


Figure 5.3 Effect of Temperature on the sensor at the light density of 20 mA, 40 mA, 80 mA and 150 mA, respectively.

In the Fig. 5.3 the effect is demonstrated indicating the operating range of the sensor when exposed to the dark currents under four different temperatures, which indicates that under the 35°C and 40°C temperature the sensor acquires the lowest possible range of resistivity due to high UV absorption in high temperature, while at 25°C and 30°C the sensor has highest range of resistivity. The plot indicates that under the LED currents, the sensor at 25°C and 30°C operates at 150000 kΩ to nearly 8000 kΩ with increasing LED current density. Under the same LED currents but with increased temperature at 35°C and 40°C, the sensor is operating in the range of 500 kΩ to 200 kΩ. This effect of temperature can be controlled by two measurement method, differential measurement, and Lock-in measurement or Lock – in amplifier. In the differential method, it is regarded as the voltage difference between the two wires, and it reduces the effect of noise, temperature etc on one wire and filter the effect through common mode rejection theory [42]. A lock-in amplifier multiplies its input by a reference signal, a process also known as down-mixing or heterodyne/homodyne detection, and then filters the output using an adjustable low-pass filter [43]. Thus, the knowledge of both the methods can be applied to reduce the temperature effect on the sensor. Two sensors can be introduced in the device, so that one sensor neutralizes the effect on the other sensor and keep the operative resistance and current at the similar range at a higher temperature without being influenced by temperature, noise, humidity etc.

5.2 Indoor Testing

The sensor has been induced in the device and in this section the performance of the device has been evaluated in indoor Thorlabs light setup to verify the results obtained by the device and compare it with the laboratory setup results as well as other UV meter results. In the [Fig. 5.5](#), the graph of the laboratory result has been demonstrated comparing the performance of the device with another established UV index meter. The UV index meter that has been taken as standard for comparison with UV index monitoring device of this project is the “Digital Ultraviolet Radiometer model 6.5” [Fig. 5.4](#).



Figure 5.4 Digital Ultraviolet Radiometer model 6.5 [41]

The Digital Ultraviolet Radiometer device calibrates the obtain UV index into numerical range between 0-11, where numerical value 1 -2 improvise low UV radiation, 3-5 moderate radiation, 6-7 high radiation, 8-10 very high radiation and more than 11 is extreme radiation. For the UV index monitoring device for this project the numerical range is determined in the [Table 5.2](#) below.

[Table 5.2](#) – UV Index Numerical Indicator

Numerical Range	UV Index	Message
0-3	Low UV	No protection required
3-5	Moderate UV	No protection required.
5-7	High UV	Protection is required.
7-10	Extreme UV	Protection required immediately.

The device has been tested in the laboratory under the LED diode with 375 nm wavelength light and device performance is satisfactory in comparison with the established Digital Ultraviolet Radiometer model 6.5. the device also performs the same nature of the simulation as such the Keithley performance where UV rise with LED turned ON and decreases with the LED turned OFF ([Fig. 5.5](#)).

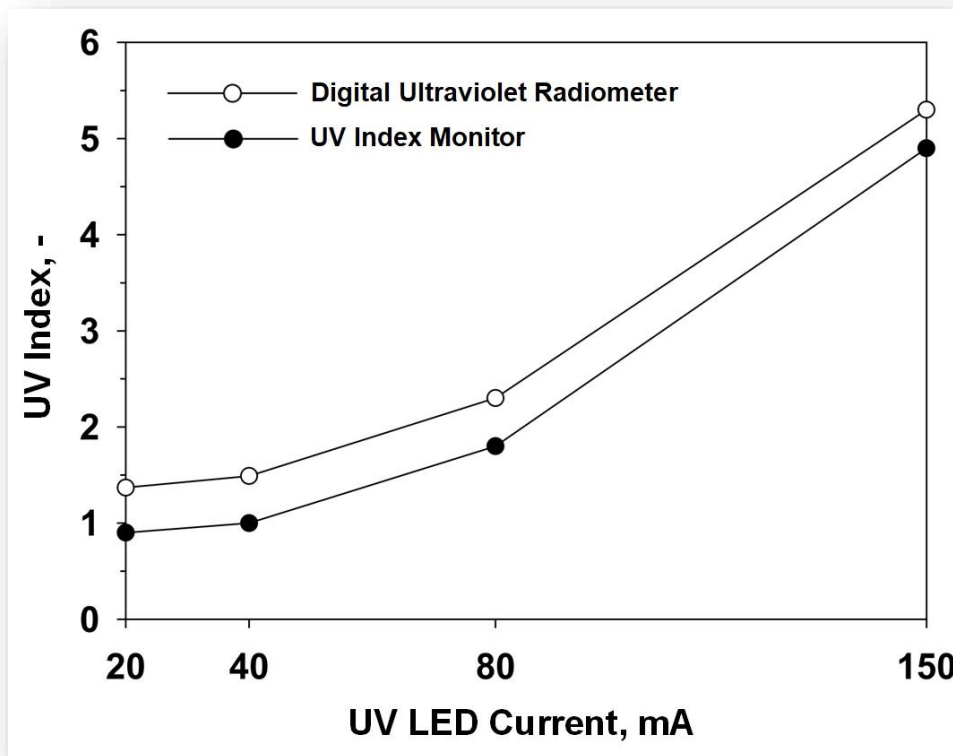


Figure 5.5 Comparison of UV index results from this device and Digital Ultraviolet Radiometer under Thorlabs light setup in the laboratory

From the [Fig. 5.5](#) it is observed that the values obtained from this project device approximately close to the values of the commercialized Digital Ultraviolet Radiometer. The test has been carried out by varying the same LED current of the laser diode of 375 nm wavelength which is 20mA, 40mA, 80mA and 150 mA such as the sensor testing procedure in the sensor testing section above in this chapter. The result from the device varies from 0.9 to around 5.0 UV index with the increment of the LED current and the commercial UV radiometer varies from around 1 to 5.3. The device performance is based on the UV nano sensor, and it can be noticed from the graph that the sensor performance has delays with LED turned ON and OFF phase. The delay in this case is nearly negligible due to the fast reaction of the sensor in this project but it can be improved with faster responsive sensor for commercial usage. Thus, the device demonstrated prominent performance in indoor testing.

5.3 Outdoor Testing

The device has been also verified under natural sunlight outdoor through different time frame of a day and carried out on a period of 7 days around possible same time of the day. The device has been mounted on the wrist like a hand watch [Fig. 5.6](#) and the UV index has been measured.

a.



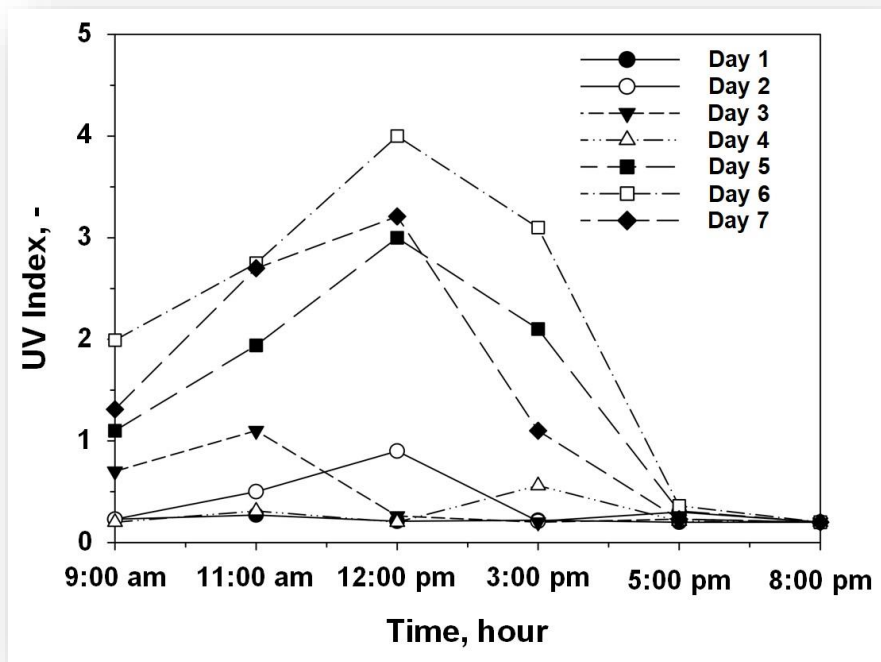
b.



Figure 5.6 UV Index Monitor

The [Fig. 5.7 a](#), indicates the graph of the performance of this device from Day -1 to Day -7 of the week demonstration of the outdoor results and [Fig.5.7 b](#), demonstrate the comparison of this device with the commercial device.

a.



b.

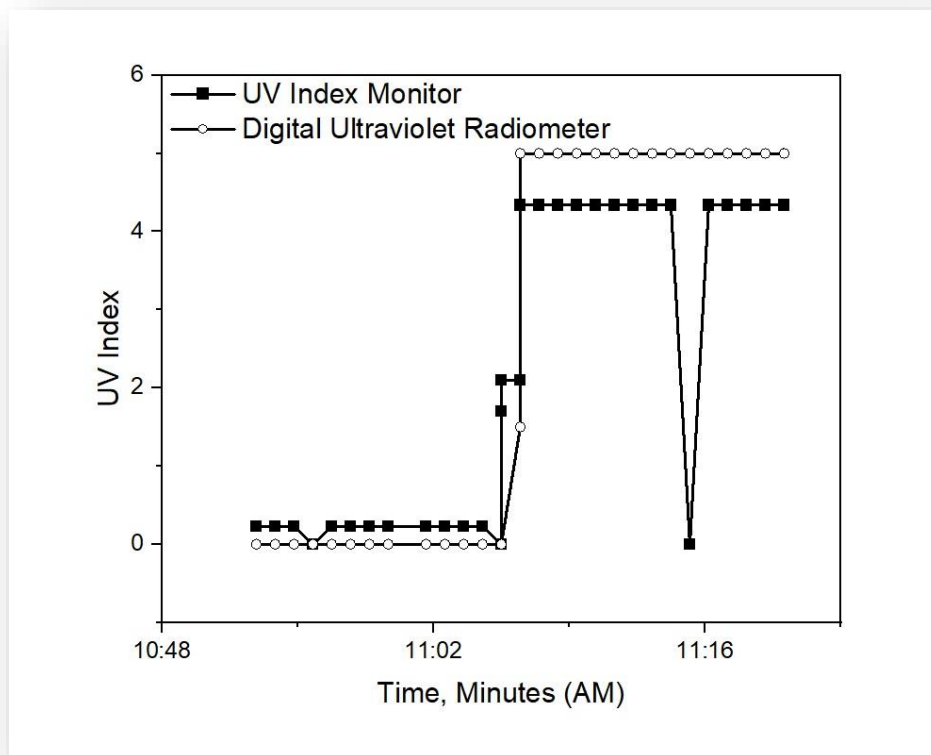


Figure 5.7 (a) 7 days outdoor UV index by this device and (b) Outdoor Comparison with Commercial UV Radiometer

In the [Fig. 5.7 a](#), the testing has been carried out around 9 am, 11 pm, 12pm, 3pm, 5pm and 8pm of seven consecutive days. The results of the 7-day UV index indicates the UV radiation detected by this device and the highest and lowest value in a particular day. The UV index has also been carried out at evening and late-night hours to verify the detection of the device accurately. In the [Table 5.3](#) below the weather details of the 7 consecutive days in Sydney during the month of June, 2022 - July, 2022 has been provided [44]. The results explain the indication of the UV index according to the standard UV index range from 0-10 respectively of those 7 consecutive days. It indicated in the [Fig. 5.7 a](#), that on rainy days or mostly rainy days the UV index is near to 0, which means no UV has been detected, whereas on slightly cloudy days or sunny days the UV index jumps from 0 to 5 index value at the specific time of exposure to natural sunlight. The outcome of this device in outdoor testing also displays prominent UV index in comparison with the commercial UV meter and thus device performance is overall effective.

[Table 5.3](#) – Weather of 7 Consecutive Days of outdoor testing in Sydney (H = Highest, L= Lowest) [44]

Day	Weather of the Day	Temperature	Sunrise	Sunset
1	Rainy Day	H: 17°C; L: 13°C	7:01 am	4:57 pm
2	Rainy Day	H: 17°C; L: 14°C	7:01 am	4:57 pm
3	Rainy Day	H: 17°C; L: 15°C	7:00 am	4:58 pm
4	Rainy Day	H: 16°C; L: 13°C	7:00 am	4:58 pm
5	Partly Sunny Day	H: 17°C; L: 14°C	7:00 am	4:59 pm
6	Mostly Sunny Day	H: 15°C; L: 8°C	7:00 am	4:59 pm
7	Cloudy	H: 16°C; L: 9°C	7:00 am	5:00 pm

In the [Fig. 5.7 b](#), another test has been graphed, with comparison between this device and the commercial device UV index around 25 mins duration in the morning period. The results from the [Fig. 5.7 b](#), indicates the detection of both the devices and UV index from both device is noticeably in a closer value range to each other. From 10:48 am to 11:02 am the devices were kept under shade, where this device indicates 0.23 value and the radiometer indicates 0, which means no presence of UV radiation. Similarly, around 11:04 am to 11:16 am the devices have been taken out to natural sunlight where, this device indicates 4.34 index and radiometer indicates 5. This device turns ON its sleep mode after every 10 minutes of operation and hence the value drops to 0 for 1 minute sleep mode of the device for power consumption. Hence the performance of UV Index Monitor is similar to the commercial radiometer with offering more technologically advance options like, sharing data, UV alert messages, wearable device etc. The approximately similar performance ensures the authenticity of the UV Index Monitor along with the assurance of safety notifications measures and the wearable feature of the device over the commercial one.

Chapter Six

Conclusion

Chapter 6 - Conclusion

Significant advancement of wearable technology has taken control of the progress of science and engineering. Development of such wearable technologies has been successfully flourished in the industrial level revolution. The nanotechnology has taken place of large-scale components and thus the device structure and design has become more compact and constrict. With the advancement of such miniature devices, the technological progress is rushing towards more improvised version of the established methodology.

In this thesis, UV index monitoring device has been demonstrated and its performance has been elaborated with graphical representation of the device performance. As stated above, the device structure is designed in the form of hand watch and the device will be mounted on the wrist of the user. The device communicates with the user through designated mobile application via Bluetooth connectivity. The device calculates UV index from 0-10 numerical range for the user to indicate the amount of UV radiation throughout a day. The device consumes low power and thus can operate 24 hours a day and 7 days a week. The device is battery operated and rechargeable which makes the device easy for the user to maintain. The device not only measures UV index for the user, but also alert the user about the UV radiation at a specific time and delivers the message of precaution necessary according to the measured UV index. The device furthermore offers the features of storing the data on a regular basis through sharing the excel data file format with different platform i.e., email etc.

The device has demonstrated satisfactory performance in comparison of the established UV photodetection devices and laboratory setup. The performance of the device has been evaluated in accordance with the effect of temperature effect, varying LED current (in the laboratory) and under natural sunlight on different days i.e., rainy days, sunny day, gloomy days etc. The ZnO based UV nano sensor has shown efficient performance in case of the sensitivity of the sensor and the photo response is impressive. The rise and fall time of the photo responsivity in the results section of the chapter 5 shows the convincing nature of the fabricated ZnO UV nano sensor with high UV sensitive behaviour and thus rapid response of the UV index at different time and environment.

Chapter Seven

Future Work

Chapter 7 – Future Work

The future work for this project has significant amount of scope for further development. The device in this project has been tested under different environmental conditions but still the durability of the device can be supervised. The device is battery operated and rechargeable. The future version of this device can be designed as self-powered version of the device or prominent power shaving mode of operation can be introduced. The dimensions and weight of the device is considered compact and miniature structure, but with more modified components it can be reduced to more and more small size. Different microcontroller, circuit designing, and calibration of the device can be achieved in the future. The device at this stage requires low power for operating the circuit but further low power can be achieved but using more advance version of microcontroller chip or introducing different circuit design for conservation of power. The device can also be modelled with different pattern of structure, such as the hand watch, can be constructed as portable credit card, high tech sunglasses etc. The core element of this device is nano UV sensor and thus the sensor can be more modified for further nano resizing and dimensions of the sensor can be decreased more. The sensor technology can also be manipulated into different and easier calculation with less complexity in precise measurement. At present, the nano sensor used in this device can be affected by humidity, temperature, atmospheric pressure, wind, precipitation, and cloudiness. The sensor can be fabricated with more advanced sensitive materials and compounds which can endure the sever factors of weather and environment. The fabrication technology of the sensor can be more modified. The materials used in this nano sensor can be evaluated time by time according to their performance and can be combine with other sensitive materials for more prominent feature. The device at present demonstrates the basic structure. The hand watch structure can be more design perfect. The space for the sensor can be more protected from outside affecting factors and the microcontroller chip can be more modified by chip designing technology. The project creates opportunities of not only nano technology and electronics rather more modified mechanical engineering can be combined for the future. The industrial level production of the device will be more exquisite and appealing in term of both outlook and technology. The device has been operating with Arduino nano 33 BLE sense, the other features of the nano board can be assembled with the device. The nano 33 BLE has different types of sensors available in the board, the UV nano sensor can be modified with the sensor properties and hence everything can be controlled withing a single microcontroller chip. The possibility of designing the device as portable is also applicable. In the end, the UV index monitoring device can be more than its current abilities. The device structure and function can be always modified, and further different miniaturized device can be produced. The device opens scope for chip design engineering which can be more beneficial in terms of wearable and functional properties.

REFERENCE

1. 2022. [Online]. Available: <https://www.cdc.gov/nceh/features/uv-radiation-safety/index.html>. [Accessed: 17- Jun- 2022].
2. "ultraviolet radiation | Definition, Examples, Effects, Wavelengths, Types, & Facts", *Encyclopedia Britannica*, 2022. [Online]. Available: <https://www.britannica.com/science/ultraviolet-radiation>. [Accessed: 18- Jun- 2022].
3. "Solar Radiation & Photosynthetically Active Radiation - Environmental Measurement Systems", *Environmental Measurement Systems*, 2022. [Online]. Available: <https://www.fondriest.com/environmental-measurements/parameters/weather/photosynthetically-active-radiation/>. [Accessed: 11- Jul- 2022].
4. "Melanoma | Causes, Symptoms & Treatments", *Cancer.org.au*, 2022. [Online]. Available: <https://www.cancer.org.au/cancer-information/types-of-cancer/melanoma>. [Accessed: 18- Jun- 2022].
5. [Online]. Available: <https://www.molemap.net.au/skin-cancer-check/australians-failing-to-get-regular-checks>. [Accessed: 11- Jul- 2022].
6. "About skin cancer", *Cancer Council NSW*, 2022. [Online]. Available: <https://www.cancercouncil.com.au/skin-cancer/about-skin-cancer/>. [Accessed: 19- Jun- 2022].
7. Ali Imran, Muhammad Sulaman, Shengyi Yang, Arfan Bukhtiar, Muhammad Qasim, Sayed Elshahat, Muhammad Saddique Akbar Khan, Ghulam Dastgeer, Bingsuo Zou, Muhammad Yousaf, Molecular beam epitaxy growth of high mobility InN film for high-performance broadband heterointerface photodetectors, *Surfaces and Interfaces*, Volume 29, 2022, 101772, ISSN 2468-0230, <https://doi.org/10.1016/j.surfin.2022.101772>. (<https://www.sciencedirect.com/science/article/pii/S2468023022000530>)
8. "Ultraviolet - Wikipedia", *En.wikipedia.org*, 2022. [Online]. Available: <https://en.wikipedia.org/wiki/Ultraviolet>. [Accessed: 21- Jun- 2022].
9. "Electromagnetic radiation - Wikipedia", *En.wikipedia.org*, 2022. [Online]. Available: https://en.wikipedia.org/wiki/Electromagnetic_radiation. [Accessed: 21- Jun- 2022].
10. "Ozone layer - Wikipedia", *En.wikipedia.org*, 2022. [Online]. Available: https://en.wikipedia.org/wiki/Ozone_layer. [Accessed: 22- Jun- 2022].
11. "The ozone layer", 2022. [Online]. Available: <https://www.awe.gov.au/environment/protection/ozone/ozone-science/ozone-layer>. [Accessed: 22- Jun- 2022].
12. "What is UV radiation?", *Cancer Council NSW*, 2022. [Online]. Available: <https://www.cancercouncil.com.au/cancer-prevention/sun-protection/understanding-uv-radiation/what-is-uv-radiation/>. [Accessed: 22- Jun- 2022].
13. "Semiconductor Science and Technology TOPICAL REVIEW Wide-bandgap semiconductor ultraviolet photodetectors", *Iopscience.iop.org*, 2022. [Online]. Available: <https://iopscience.iop.org/article/10.1088/0268-1242/18/4/201>. [Accessed: 22- Jun- 2022].
14. "Nanoarchitectonics of Visible-Blind Ultraviolet Photodetector Materials: Critical Features and Nano-Microfabrication", *ADVANCED OPTICAL MATERIALS*, 2022. [Online]. Available: <https://onlinelibrary.wiley.com/doi/full/10.1002/adom.201800580>. [Accessed: 22- Jun- 2022].
15. Kai Ti Low, Fong Kwong Yam, Khi Poay Beh, Asrulnizam Abd Manaf, Khi Khim Beh, Characteristics and Sensing of Sol-gel derived Titanium Dioxide-based Ultraviolet Photodetector on Flame Retardant-4 Board, *Sensors and Actuators A: Physical*, Volume 323, 2021, 112654, ISSN 0924-4247, <https://doi.org/10.1016/j.sna.2021.112654>. (<https://www.sciencedirect.com/science/article/pii/S0924424721001163>)
16. Q. Ye *et al.*, "Research and Progress of Transparent, Flexible Tin Oxide Ultraviolet Photodetector", *Crystals*, vol. 11, no. 12, p. 1479, 2021. Available: 10.3390/cryst11121479.
17. C. Lin *et al.*, "Diamond based photodetectors for solar-blind communication", *Optics Express*, vol. 27, no. 21, p. 29962, 2019. Available: 10.1364/oe.27.029962.

18. Ultrahigh Sensitivity Graphene/Nanoporous GaN Ultraviolet Photodetectors, Jing Li, Xin Xi, Shan Lin, Zhanhong Ma, Xiaodong Li, and Lixia Zhao, *ACS Applied Materials & Interfaces* 2020 12 (10), 11965-11971, DOI: 10.1021/acsami.9b22651
19. Mustafa A. Yildirim, Kasif Teker, Self-powered fine-pattern flexible SiC single nanowire ultraviolet photodetector, *Journal of Alloys and Compounds*, Volume 868, 2021, 159255, ISSN 0925-8388, <https://doi.org/10.1016/j.jallcom.2021.159255>. (<https://www.sciencedirect.com/science/article/pii/S0925838821006630>)
20. Liu, K., Sakurai, M., & Aono, M. (2010). ZnO-based ultraviolet photodetectors. *Sensors (Basel, Switzerland)*, 10(9), 8604–8634. <https://doi.org/10.3390/s100908604>
21. B. Deka Boruah, "Zinc oxide ultraviolet photodetectors: rapid progress from conventional to self-powered photodetectors", *Nanoscale Advances*, vol. 1, no. 6, pp. 2059-2085, 2019. Available: 10.1039/c9na00130a.
22. Basavaraj G. Hunashimarad, J.S. Bhat, P.V. Raghavendra, R.F. Bhajantri, ZnO:Ca MSM ultraviolet photodetectors, *Optical Materials*, Volume 124, 2022, 111960, ISSN 0925-3467, <https://doi.org/10.1016/j.optmat.2021.111960>. (<https://www.sciencedirect.com/science/article/pii/S0925346721011605>)
23. *In Situ* Fabrication of PdSe₂/GaN Schottky Junction for Polarization-Sensitive Ultraviolet Photodetection with High Dichroic Ratio, Di Wu, Mengmeng Xu, Longhui Zeng, Zhifeng Shi, Yongzhi Tian, Xin Jian Li, Chong-Xin Shan, and Jiansheng Jie, *ACS Nano* 2022 16 (4), 5545-5555. DOI: 10.1021/acsnano.1c10181
24. H. B., S. K. P. and N. K. N., "Low temperature-processed ZnO thin films for p–n junction-based visible-blind ultraviolet photodetectors", *RSC Advances*, vol. 8, no. 65, pp. 37365-37374, 2018. Available: 10.1039/c8ra07312k.
25. "biotechnology | Definition, Examples, & Applications", *Encyclopedia Britannica*, 2022. [Online]. Available: <https://www.britannica.com/technology/biotechnology>. [Accessed: 30- Jun- 2022].
26. P. Cvetelin Vasilev, "Nanofabrication: Techniques and Industrial Applications", *AZoNano.com*, 2022. [Online]. Available: <https://www.azonano.com/article.aspx?ArticleID=5876>. [Accessed: 30- Jun- 2022].
27. F. Meierhofer, L. Mädler and U. Fritsching, "Nanoparticle evolution in flame spray pyrolysis—Process design via experimental and computational analysis", *AIChE Journal*, vol. 66, no. 2, 2019. Available: 10.1002/aic.16885.
28. W. Teoh, R. Amal and L. Mädler, "Flame spray pyrolysis: An enabling technology for nanoparticles design and fabrication", *Nanoscale*, vol. 2, no. 8, p. 1324, 2010. Available: 10.1039/c0nr00017e.
29. Betancourt T, Brannon-Peppas L. Micro- and nanofabrication methods in nanotechnological medical and pharmaceutical devices. *Int J Nanomedicine*. 2006;1(4):483-95. doi: 10.2147/nano.2006.1.4.483. PMID: 17722281; PMCID: PMC2676643.
30. D. Sumanth Kumar, B. Jai Kumar, H.M. Mahesh, Chapter 3 - Quantum Nanostructures (QDs): An Overview, Editor(s): Sneha Mohan Bhagyaraj, Oluwatobi Samuel Oluwafemi, Nandakumar Kalarikkal, Sabu Thomas, In *Micro and Nano Technologies, Synthesis of Inorganic Nanomaterials*, Woodhead Publishing, 2018, Pages 59-88, ISBN 9780081019757, <https://doi.org/10.1016/B978-0-08-101975-7.00003-8>. (<https://www.sciencedirect.com/science/article/pii/B9780081019757000038>)
31. G. Osenga, "Dry Etching and Wet Etching", *Thierry-corp.com*, 2022. [Online]. Available: <https://www.thierry-corp.com/plasma-knowledgebase/dry-etching-and-wet-etching>. [Accessed: 11- Jul- 2022].
32. "Thin-film Electrochemical Sensors | MicruX", *Micruxfluidic.com*, 2022. [Online]. Available: <https://www.micruxfluidic.com/en/shop/electrochemical-solutions/thin-film-electrochemical-sensors/?p=all#desc-19>. [Accessed: 11- Jul- 2022].
33. "Product Catalog - Thorlabs", *Thorlabs.com*, 2022. [Online]. Available: https://www.thorlabs.com/navigation.cfm?guide_id=1. [Accessed: 13- Jul- 2022].
34. "Arduino Nano 33 BLE Sense", *Arduino Online Shop*, 2022. [Online]. Available: <https://store-usa.arduino.cc/products/arduino-nano-33-ble-sense>. [Accessed: 04- Jul- 2022].

35. "BLE- An overview", *Medium*, 2022. [Online]. Available: <https://medium.com/@muhamed.riyas/ble-an-overview-d524ceb73c94>. [Accessed: 04- Jul- 2022].
36. 2022. [Online]. Available: <https://www.te.com/usa-en/plp/resistors/Y30xv.html>. [Accessed: 13- Jul- 2022].
37. P. 120mAh, "Polymer Lithium Ion Battery (LiPo) 3.7 V 120mAh", *Core-electronics.com.au*, 2022. [Online]. Available: <https://core-electronics.com.au/lipo-polymer-lithium-ion-battery-120mah.html>. [Accessed: 13- Jul- 2022].
38. A. v1, "Adafruit Micro Lipo w/MicroUSB Jack - USB LiIon/LiPoly charger - v1", *Core-electronics.com.au*, 2022. [Online]. Available: <https://core-electronics.com.au/adafruit-micro-lipo-w-microusb-jack-usb-liion-lipoly-charger-v1.html>. [Accessed: 13- Jul- 2022].
39. S. Switch, "SPDT Slide Switch", *Core-electronics.com.au*, 2022. [Online]. Available: <https://core-electronics.com.au/spdt-slide-switch.html>. [Accessed: 13- Jul- 2022].
40. 2022. [Online]. Available: https://au.element14.com/multicomp-pro/mcte1-199131-s/peltier-module-200w-50-x-50-x/dp/1639732?CMP=KNC-GAU-GEN-DSA-RLSA-PUR-BS-IS&mckv=s_dc|pcrid|418991129172|pkw||pmt||slid||product||pgrid|18902993568|ptaid|aud-291708565361:dsa-82306211808|&gclid=EAIaIQobChMIpNzwr3x-AIVmQsrCh1MIQluEAAYASAAEgIElfD_BwE. [Accessed: 11- Jul- 2022].
41. "Solarmeter 6.5 UV Index Meter", *Solarmeter.com.au*, 2022. [Online]. Available: <http://www.solarmeter.com.au/model65.html>. [Accessed: 11- Jul- 2022].
42. "Differential vs. Single-ended Measurements", *Apogeeinstruments.com*, 2022. [Online]. Available: <https://www.apogeeinstruments.com/differential-vs-single-ended-measurements/#:~:text=The%20measurement%20is%20taken%20as,of%20the%20data%20acquisition%20system>. [Accessed: 13- Jul- 2022].
43. "Principles of Lock-in Detection", *Zurich Instruments*, 2022. [Online]. Available: <https://www.zhinst.com/others/en/resources/principles-of-lock-in-detection>. [Accessed: 13- Jul- 2022].
44. Past Weather in Sydney, New South Wales, Australia — Yesterday or Further Back", *Timeanddate.com*, 2022. [Online]. Available: <https://www.timeanddate.com/weather/australia/sydney/historic>. [Accessed: 14- Jul- 2022].

APPENDIX – I

Arduino Code:

```
#include <ArduinoBLE.h>
#include <Arduino_HTS221.h>
BLEService uvService("19B10000-E8F2-537E-4F6C-D104768A1214");
BLEFloatCharacteristic uvCharacteristic("19B10001-E8F2-537E-4F6C-D104768A1214", BLERead |
BLEWrite | BLENotify);
BLEByteCharacteristic msgCharacteristic("19B10002-E8F2-537E-4F6C-D104768A1214", BLERead |
BLEWrite | BLENotify);
BLEFloatCharacteristic rCharacteristic("19B10003-E8F2-537E-4F6C-D104768A1214", BLERead |
BLEWrite | BLENotify);

BLEService moreService("E55B9A96-3B82-4CE0-AADE-D21792165351");
BLEFloatCharacteristic vCharacteristic("A5CAA74-35AD-4F03-938E-2E4937E0D26B", BLERead |
BLEWrite | BLENotify);
BLEFloatCharacteristic tCharacteristic("F3766E70-FBF1-4BEB-ABEB-1C12A819AC44", BLERead |
BLEWrite | BLENotify);
BLEFloatCharacteristic hCharacteristic("2F6BE2DC-E39D-499C-A652-8FDC1D87A79D", BLERead |
BLEWrite | BLENotify);

int analogPin = A0;
int raw = 0;
int Vin = 3.3;
float Vout = 0;
float R1 = 220;
float R2 = 0;
float buffer = 0;
int avg_tracker=0;
int avg_array[10];

int wakeTime = 10; // sensor reading time in minute
int sleepTime = 1 ; // sleep time in minute

int dcount = 0;
int dcountMax = 210;

void setup() {
  Serial.begin(9600);

  pinMode(analogPin, INPUT);
  //digitalWrite(LED_PWR, LOW);

  if (!HTS.begin()) {
    Serial.println("Failed to initialize humidity temperature sensor!");
    while (1);
  }
}
```

```

}

// begin initialization
if (!BLE.begin()) {
  Serial.println("starting BLE failed!");

  while (1);
}

// set advertised local name and service UUID:
BLE.setLocalName("My UV Sensor");
BLE.setAdvertisedService(uvService);

// add the characteristic to the service
uvService.addCharacteristic(uvCharacteristic);
uvService.addCharacteristic(msgCharacteristic);
uvService.addCharacteristic(vCharacteristic);
moreService.addCharacteristic(rCharacteristic);
moreService.addCharacteristic(tCharacteristic);
moreService.addCharacteristic(hCharacteristic);

// add service
BLE.addService(uvService);
BLE.addService(moreService);

// set the initial value for the characteristic:
uvCharacteristic.writeValue(0.0);
rCharacteristic.writeValue(0.0);
vCharacteristic.writeValue(0.0);
tCharacteristic.writeValue(0.0);
hCharacteristic.writeValue(0.0);

// start advertising
BLE.advertise();

Serial.println("BLE Peripheral");
}

void loop() {
  // listen for BLE peripherals to connect:
  BLEDevice central = BLE.central();

  // if a central is connected to peripheral:
  if (central) {
    Serial.print("Connected to central: ");
    // print the central's MAC address:
    Serial.println(central.address());

    // while the central is still connected to peripheral:
    while (central.connected()) {

```

```

float _temperature = HTS.readTemperature();
float _humidity = HTS.readHumidity();
// print each of the sensor values
Serial.print("Temperature = ");
Serial.print(_temperature);
Serial.println(" °C");

Serial.print("Humidity = ");
Serial.print(_humidity);
Serial.println(" %");

// print an empty line
Serial.println();

/* actual nano 33 firmware code STARTS */
tCharacteristic.writeValue(_temperature);
hCharacteristic.writeValue(_humidity);
raw = analogRead(analogPin);
if (raw)
{
  //buffer = raw * Vin;
  Vout = map(raw, 0,1024,0,3.3);
  //buffer = (Vin / Vout) - 1;
  R2 = (Vout * R1) / (Vin - Vout) ;
  Serial.print("Vout: ");
  Serial.println(Vout);
  Serial.print("R2: ");
  Serial.println(R2);
  rCharacteristic.writeValue(R2);
  vCharacteristic.writeValue(Vout);

  digitalWrite(LED_PWR, HIGH); //led ON, wakeup

  delay(1000);
  float uvIntensity = mapfloat(raw, 650, 1024, 10, 0);
  //(InputValue, input min, input max, mapped min, mapped max)

  Serial.print("uvIntensity:");
  Serial.println(uvIntensity/10);

  uvCharacteristic.writeValue(uvIntensity/10); // without avg

  //for power saving mode

  dcount++;

  if(dcount>=dcountMax){
    Serial.println("sleep mode");
    rCharacteristic.writeValue(0);
    vCharacteristic.writeValue(0);
    uvCharacteristic.writeValue(0);
  }
}

```

```
tCharacteristic.writeValue(0);
hCharacteristic.writeValue(0);
msgCharacteristic.writeValue(1);
digitalWrite(LED_PWR, LOW); //led Off
delay(sleepTime * 1000*60 ); //sleep timer
```

```
dcount = 0;
Serial.println("I woke Up");
msgCharacteristic.writeValue(0);
}
```

```
Serial.println(dcount);
}
}
/* actual nano 33 firmware code ENDS */
}
```

```
// when the central disconnects, print it out:
Serial.print(F("Disconnected from central: "));
Serial.println(central.address());
}
```

```
float mapfloat(float x, float in_min, float in_max, float out_min, float out_max) {
return (x - in_min) * (out_max - out_min) / (in_max - in_min) + out_min;
}
```